

# Decoding Topological Subsystem Color Codes Over the Erasure Channel using Gauge Fixing

Hiteshvi Manish Solanki and Pradeep Kiran Sarvepalli

*Department of Electrical Engineering, Indian Institute of Technology Madras, Chennai 600 036, India*

(Dated: November 29, 2021)

Topological subsystem color codes (TSCCs) are an important class of topological subsystem codes that allow for syndrome measurement with only 2-body measurements. It is expected that such low complexity measurements can help in fault tolerance. While TSCCs have been studied over depolarizing noise model, their performance over the erasure channel has not been studied as much. In this paper, we propose two erasure decoders for topological subsystem color codes. These decoders use the technique of gauge fixing where some of the gauge operators of the subsystem code are promoted to stabilizers. With partial gauge fixing we obtained a threshold of 17.7% on a TSCC derived from the square octagon lattice. Using an order maximal gauge fixing decoder we were able to improve the threshold to 44%. The previously known decoder for TSCC over the erasure channel had a threshold of 9.7%. We also study the correctability of erasures on the subsystem codes.

## I. INTRODUCTION

Subsystem codes are an important generalization of stabilizer codes [1–3]. One of the motivations for this generalization was to simplify the error recovery process of quantum codes. Specifically, they can simplify the syndrome computation which involves the measurement of the stabilizer generators. Intuitively, we expect that a measurement involving fewer qubits is likely to be more robust than a measurement involving many qubits. While the natural approach would be to minimize the number of qubits participating in each check, subsystem codes offer an additional degree of freedom. Subsystem codes enable the reconstruction of the syndrome, i.e., the outcome of the stabilizer measurements, with smaller measurements. The Bacon-Shor codes, for instance, allow for the measurement of stabilizers with only two body operators [1]. However, their stabilizers are global. In contrast, the topological subsystem color codes have local stabilizer generators while allowing for two body measurements for reconstructing the syndrome, [4].

Most of the studies on the performance of topological subsystem codes [5–8] focused on the depolarizing channel. The error correcting capabilities of TSCCs for handling leakage errors were explored in [9]. In contrast, the performance of TSCCs over the quantum erasure channel [10], which can be used to model qubit loss, has not been studied as much. Motivated by this gap, we began the study of topological subsystem color codes over the erasure channel and reported some preliminary results in [11]. Therein we proposed multiple two-stage erasure decoders for the TSCC derived from the square octagon lattice. Using a combination of various techniques including peeling and clustering we were able to achieve a threshold of 9.7% in [11] for the TSCC derived from the square octagon lattice. However, this threshold was not optimal and there was room for improvement.

In this paper, we continue our study of TSCCs over the erasure channel and present new decoding algorithms that improve upon the decoders in [11]. A driving force for this work is to improve the threshold of the TSCCs for erasure noise while also retaining the advantage of the subsystem codes, namely the ability to measure the syndromes using only 2-body measurements. Topological subsystem color codes have fewer stabilizer generators than a comparable color code or a

surface code. This will lead to lower thresholds [5, 6, 12]. To address this we use the technique of gauge fixing, wherein we promote some of the gauge operators to checks. Gauge fixing in effect leads to a larger stabilizer. This technique of promoting some gauge operators to stabilizers was used for analyzing the structure of subsystem codes in [5], and for quantum computation in [13, 14]. More recently, it was also employed for decoding subsystem codes [8].

There are a few challenges to overcome before gauge fixing can be useful for error correction. The additional stabilizer generators may not be measurable using 2-body measurements. It is not enough if the additional stabilizer generators are individually measurable using 2-body measurements. They must also be jointly measurable using 2-body measurements. One of the contributions of the paper is to enable gauge fixing for TSCCs while also keeping the measurements to 2-body operators. This allowed us to improve the threshold significantly over our previous work.

However, this falls short of the thresholds of the color codes and surface codes [15–17]. We then employed near complete gauge fixing to improve the threshold. A challenge in this context is to increase the number of checks while ensuring that they have a decomposition in terms of gauge measurements involving fewer qubits than the direct measurement of those checks. In addition, we also need to keep the number of measurements per check small, otherwise it could also lead to a degradation in performance when we consider faulty syndrome measurements. A novel contribution of this paper is to provide such decompositions for the additional checks used for gauge fixing. In these decompositions, we only require 2-body measurements for half the checks and 4-body measurements for the remaining half. With these results in hand, we then make use of the mapping between TSCCs and color codes to decode TSCCs.

We briefly summarize our main contributions below.

- (i) First, we propose a decoder that uses partial gauge fixing for TSCC. We obtain a threshold of 17.7% for TSCC derived from the square octagon lattice.
- (ii) We then propose an alternate “order” maximal gauge fixing decoder to improve the threshold. This decoder leads to a threshold of threshold 44%. This improvement is attained at the expense of a slight increase in complexity.
- (iii) We give an explicit decomposition of the stabilizers of

the color codes in terms of 2-body and 4-body gauge operators.

(iv) We study the correctability of erasures on a subsystem code. Specifically, we provide a necessary and sufficient condition for an erasure pattern to be correctable on a subsystem code (without gauge fixing). We also study correctability of erasures under the order maximal gauge fixing decoder.

Along the way, we provide additional insight into the mapping between TSCCs and copies of the parent color code [5]. These results could be independent interest.

There are two related works in addition to our previous work [11]. In [9], the authors studied topological subsystem codes for correcting leakage errors, a more severe form of noise than erasure noise. While somewhat related, this noise model is different from ours and assumes that the locations of the erased qubits are unknown.

With respect to the technique of gauging fixing, the closest work is that of [8] where the authors also uses gauge fixing for decoding subsystem codes. There are important differences between our work and theirs. We mention some of them below. First of all, the noise models are different. We consider erasure noise while they consider depolarizing noise and biased noise models. Secondly, we study topological subsystem color codes, while they consider subsystem surface codes and their generalizations over hyperbolic surfaces. Thirdly, for the class of codes we consider, single qubit errors lead to three nonzero syndromes while the class of codes considered in [8] assume a pair of nonzero syndromes. This difference is fundamental as the decoding algorithms of [8] are not applicable to the class of codes we study. Fourthly, note that TSCCs are non-CSS codes while the codes studied in [8] are CSS codes. Another important difference is that in our decoding algorithms the 2-body generators of the gauge group are not treated as stabilizers, i.e., their measurements are not used as syndromes. This is in contrast to the approach in [8] where the gauge generators are also treated as intermediate stabilizers. In our approach the gauge measurements are either 2-body or 4-body while in [8], they are 3-body operators.

We organize the paper as follows. In Section II we review the background for our proposed decoders. In Section III we give an overview of the proposed decoding algorithms. Section IV discusses the first stage for  $X$  error correction and Section V discusses the second stage for  $Z$  error correction. Then we discuss some theoretical bounds for the number of correctable erasures on TSCC in Section VI. We report the simulation results in Section VII and finally conclude with a brief summary in Section VIII.

## II. BACKGROUND

In this section, we briefly review some background material. We assume that the reader is familiar with stabilizer codes, see [18, 19] for an introduction.

### A. Subsystem codes

We briefly review subsystem codes. For more details we refer the reader to [19]. Subsystem codes are obtained from stabilizer codes by not encoding information in some of the logical qubits. These qubits are called the gauge qubits. Any error on the gauge qubits do not affect the codespace. An  $[[n, k, r, d]]$  subsystem code encodes  $k$  logical qubits and  $r$  gauge qubits into  $n$  qubits. It can detect errors upto  $d - 1$  qubits, where  $d$  is the distance of the code. The distance also signifies the smallest weight of non-trivial logical operator.

We define a subsystem code by a subgroup  $\mathcal{G} \subset \mathcal{P}_n$ , where  $\mathcal{P}_n$  is the Pauli group on  $n$  qubits. Elements of  $\mathcal{G}$  are called the *gauge operators*. Elements which generate the gauge group are called the *gauge generators*. Recall that the centralizer of a subgroup  $\mathcal{G} \subseteq \mathcal{P}_n$  is defined as

$$C(\mathcal{G}) = \{g \in \mathcal{P}_n \mid gh = hg \text{ for all } h \in \mathcal{G}\} \quad (1)$$

The *stabilizer*  $\mathcal{S}$  of the subsystem code is a subgroup of  $\mathcal{G}$  such that  $\langle iI, \mathcal{S} \rangle = \mathcal{G} \cap C(\mathcal{G})$ , where  $C(\mathcal{G})$  is the centralizer of  $\mathcal{G}$ . Elements of  $\mathcal{S}$  act trivially on the code space. It is convenient to ignore the phases and write the stabilizer up to a phase as follows.

$$\mathcal{S} = \mathcal{G} \cap C(\mathcal{G}) \quad (2)$$

Since  $\mathcal{S} \subseteq \mathcal{G}$ , it follows that

$$\mathcal{S} \subseteq \mathcal{G} \subseteq C(\mathcal{G}) \subseteq C(\mathcal{S}). \quad (3)$$

For an  $[[n, k, r, d]]$  subsystem code, ignoring phases, there are  $2r + s$  independent generators for  $\mathcal{G}$  and  $s$  independent generators for  $\mathcal{S}$ , where  $n = k + r + s$ , see [3]. Operators in  $C(\mathcal{G}) \setminus \mathcal{G}$  are called bare logical operators while operators in  $C(\mathcal{S}) \setminus \mathcal{G}$ , obtained by appending gauge operators to the bare logical operators, are called dressed logical operators, see [6].

### B. Topological color codes

Topological color codes (TCCs) in 2D are defined on lattices where the vertices are trivalent and faces are 3-colorable [20]. These lattices are also called 2-colexes. A quantum code can be defined on 2-colex by placing qubits on the vertices, and checks on faces. (We can shall refer to a 2-colex as a color code for this reason). For any face  $f$ , a pair of stabilizers are defined as follows:

$$B_f^X = \prod_{v \in f} X_v \text{ and } B_f^Z = \prod_{v \in f} Z_v \quad (4)$$

where  $X$  and  $Z$  are the Pauli matrices. Let  $f_\gamma$  be set of faces of  $\gamma$  color,  $\gamma \in \{r, g, b\}$ . These checks satisfy the following relations:

$$\prod_{f \in f_r} B_f^Z = \prod_{f \in f_g} B_f^Z = \prod_{f \in f_b} B_f^Z \quad (5a)$$

$$\prod_{f \in f_r} B_f^X = \prod_{f \in f_g} B_f^X = \prod_{f \in f_b} B_f^X \quad (5b)$$

This equality depicts that there are four dependencies among the stabilizer generators given in Eq. (4). A color code defined on a 2-colex embedded on a surface of genus  $g$  encodes  $4g$  qubits. For the rest of the paper we assume that the color code is defined on a torus which has genus one. In this case the color code encodes 4 logical qubits.

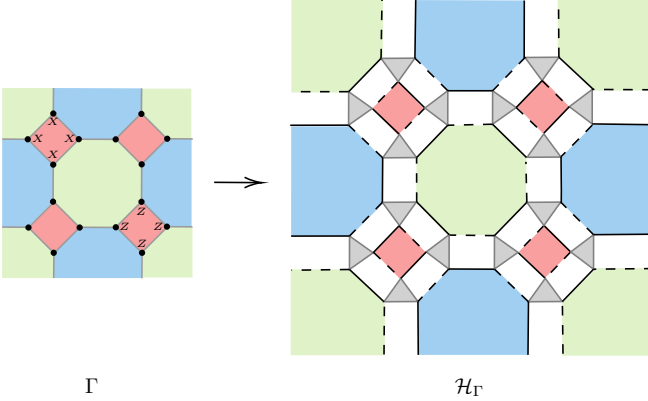


FIG. 1: The figure on left shows the color code defined on 2-colex. Solid dots indicate the qubits. Every face has a  $X$  type stabilizer and a  $Z$  type stabilizer associated to it. A hypergraph  $\mathcal{H}_\Gamma$  can be constructed from this 2-colex. The hypergraph is depicted on the right. Shaded triangles correspond to rank-3 edges. A TSCC is defined on this hypergraph. Qubits are located on the vertices of the hypergraph and its edges define the gauge group of the TSCC as in Eq. (7).

### C. Topological subsystem color codes

Topological subsystem color codes (TSCCs) are a class of subsystem codes obtained from TCCs [4]. To construct a TSCC, we construct a hypergraph from the 2-colex on which the color code is defined. Recall that the hypergraph is defined by an ordered pair  $(V, E)$  where  $V$  is the set of vertices of the hypergraph and  $E$ , called edges of the hypergraph, is a collection of subsets of  $V$ . First, we replace every TCC vertex with a triangle. The three vertices of triangle form a rank-3 edge. If  $u, v, w$  are the vertices of the triangle, then the corresponding rank-3 edge is denoted  $(u, v, w)$ . These newly formed vertices are denoted  $V$ . Next we split every edge to two edges: solid and dashed, placed in alternating fashion around each triangle, see Fig. 1. These newly formed edges are called rank-2 edges. The resulting object is a hypergraph as shown in [6]. The collection of rank-2 edges is denoted  $E_2$  while the set of rank-3 edges is denoted  $E_3$ . Together they constitute  $E = E_2 \cup E_3$ , the edges of the hypergraph. The hypergraph is now defined by the ordered pair  $(V, E)$ .

Faces are somewhat more complicated to define. Each face of the color code gives rise to a face in the hypergraph. It also inherits the color from the underlying face in the 2-colex. We denote these faces by  $F$ . The  $c$  colored faces are denoted  $F_c$ . Note that  $F = F_r \cup F_g \cup F_b$ . Vertex expansion of the 2-colex also creates 4-sided faces on the hypergraph which are denoted by  $F_4$ . Each such 4-sided face is bounded by two

rank-2 edges and two rank-3 edges. The rank-2 edges belong to faces of different color. We denote by  $F_{cc'}$  the set of all such faces which are between faces  $f_c \in F_c$  and  $f_{c'} \in F_{c'}$ .

One can construct a subsystem code from the hypergraph obtained from the 2-colex as follows, see [4, 6]. Place qubits on the vertices of the hypergraph and for each rank-2 edge of the hypergraph we associate a Pauli operator. Every rank-3 edge  $e = (u, v, w)$  is also assigned an operator  $K_e = Z_u Z_v Z_w$ . Note that for each rank-3 edge  $(u, v, w)$  we define three  $ZZ$  operators for each pair of vertices, namely,  $Z_u Z_v$ ,  $Z_v Z_w$  and  $Z_u Z_w$ . Of these three  $ZZ$  operators only two are independent. These 2-body  $ZZ$  operators along with the rank-2 edge operators generate the gauge group of the TSCC. (Note that the operator  $Z_u Z_v Z_w$  is not a gauge operator.) If a pair of vertices  $e = (u, v)$  form a rank-2 edge or belong to a rank-3 edge we define

$$K_e = K_{(u, v)} = \begin{cases} X_u X_v & (u, v) \text{ is dashed edge} \\ Y_u Y_v & (u, v) \text{ is solid edge} \\ Z_u Z_v & (u, v) \text{ is in some hyperedge} \end{cases} \quad (6)$$

We can then define the gauge group of the subsystem code as follows.

$$\mathcal{G} = \langle K_{(u, v)} \mid (u, v) \text{ are adjacent} \rangle \quad (7)$$

The stabilizers and the logical operators of the TSCC are completely determined by the gauge group. In case of TSCCs, they can be characterized in terms of cycles of the hypergraph.

A cycle in a hypergraph is a collection of edges such that every vertex has an even degree with respect to these edges. A rank-2 cycle involves only rank-2 edges. A hypercycle involves both rank-2 edges and hyperedges (rank-3 edges). To every cycle  $\sigma$  we can associate a operator as follows.

$$W(\sigma) = \prod_{e \in \sigma} K_e \quad (8)$$

The importance of these operators is that they are precisely the operators in  $C(\mathcal{G})$ , the centralizer of  $\mathcal{G}$ . A generating set for  $C(\mathcal{G})$  can be given by considering all the cycles. Cycles of trivial homology generate the stabilizer of the TSCC while cycles of nontrivial homology give rise to the logical operators of the TSCC. Fig. 2 shows cycles of trivial homology which correspond to stabilizers while Fig. 3 shows cycles of nontrivial homology which correspond to the (bare) logical operators on TSCC defined on the hypergraph derived from the square octagon lattice.

For every face  $f \in F$ , we associate two independent cycles:

- i) A rank-2 cycle denoted  $\sigma_1^f$ . This is formed by the rank-2 edges in the boundary of  $f$ .
- ii) A hypercycle denoted  $\sigma_2^f$ . This is formed by the rank-2 as well as rank-3 edges in the boundary of  $f$ .

(A dependent hypercycle can be generated by  $\sigma_1^f$  and  $\sigma_2^f$ .) The hypercycle  $\sigma_2^f$  is chosen so that the edges corresponding to the  $XX$  type gauge operators in the boundary of  $f$  are chosen to be in the hypercycle, see Fig. 2. Cycles of trivial homology correspond to stabilizer generators of the subsystem code. We

denote the stabilizer from rank-2 cycles as  $W_1^f$  and the stabilizer from the hypercycle as  $W_2^f$ .

$$W_1^f = \prod_{e \in \sigma_1^f} K_e = \prod_{v \in f} Z_v \quad (9a)$$

$$W_2^f = \prod_{e \in \sigma_2^f} K_e = \prod_{(u, v, w) \in f} X_u Y_v Y_w, \quad (9b)$$

where  $K_e$  is the edge operator associated to the edge  $e$ . The alternate forms simply follow by substituting for the edge operators  $K_e$ . Fig. 2 shows these stabilizers:  $W_1$  on faces  $f_1$  and  $f_2$  and  $W_2$  on faces  $f_3$  and  $f_4$ .

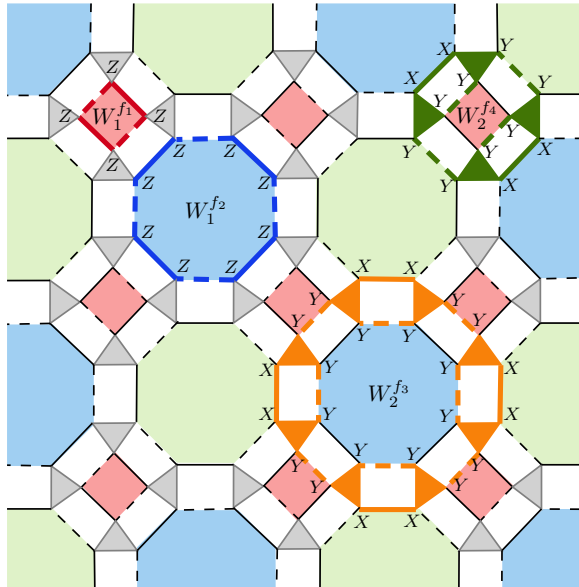


FIG. 2: Subsystem code defined on square octagon lattice. Also shown are the cycles and the associated stabilizers (in color). Every face has a  $Z$  type stabilizer coming from the rank-2 cycle, see  $W_1^{f_1}$  and  $W_1^{f_2}$ . Every face also has a stabilizer attached to a hypercycle, see  $W_2^{f_3}$  and  $W_2^{f_4}$ . This stabilizer is neither  $X$  type nor  $Z$  type.

The following dependencies exist among the stabilizer generators of the topological subsystem color codes on a torus.

$$\prod_{f \in \mathcal{F}_r} W_2^f \prod_{f \in \mathcal{F}_g} W_2^f = \prod_{f \in \mathcal{F}_b} W_1^f \prod_{f \in \mathcal{F}_r} W_1^f \quad (10a)$$

$$\prod_{f \in \mathcal{F}_r} W_2^f \prod_{f \in \mathcal{F}_b} W_2^f = \prod_{f \in \mathcal{F}_g} W_1^f \prod_{f \in \mathcal{F}_b} W_1^f \quad (10b)$$

The above relations show that there are  $s = 2|\mathcal{F}| - 2$  independent stabilizer generators for the TSCC assuming that there are  $|\mathcal{F}|$  faces.

**Remark 1.** When defined on a torus we can show that the number of qubits is  $n = 6|\mathcal{F}|$ . The number of independent gauge generators is given by  $2r + s = 10|\mathcal{F}| - 2$ , where  $r$  is the number of gauge qubits which gives us  $r = 4|\mathcal{F}|$ . The number of encoded qubits is  $k = 2$ .

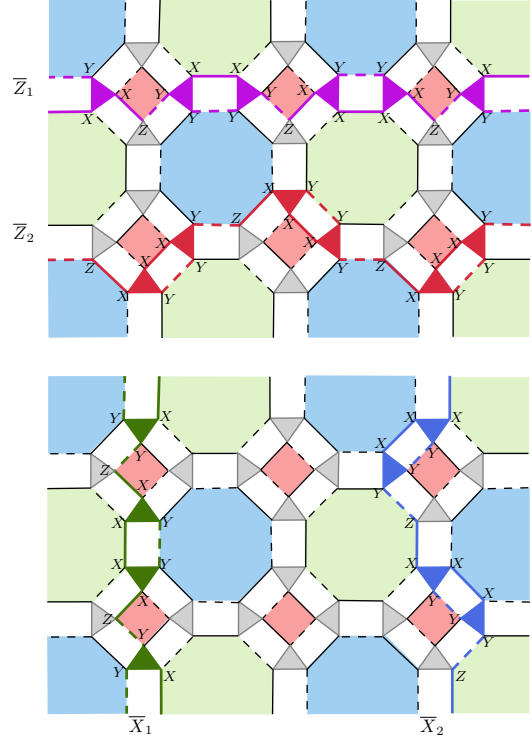


FIG. 3: Cycles of nontrivial homology which correspond to the logical operators (in color). There are four bare logical operators  $\bar{X}_1, \bar{X}_2, \bar{Z}_1, \bar{Z}_2$  for TSCC defined on square octagon lattice with periodic boundary conditions.

Furthermore, from the theory of TSCCs we know that each of the stabilizer generators  $W_1^f$  and  $W_2^f$  can be decomposed as a product of  $O(|f|)$  gauge operators. This decomposition is shown in Fig. 4.

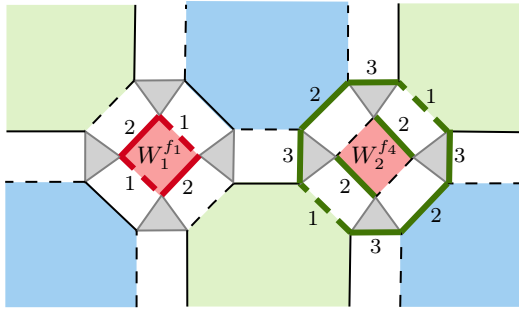


FIG. 4: Decomposition of rank-2 stabilizer  $W_1^{f_1}$  and hypercycle stabilizer  $W_2^{f_4}$  in terms of the 2-body gauge operators. The labels on the edges indicate the sequence in which the gauge operators are measured.

As mentioned, the stabilizer generators  $W_1^f$  and  $W_2^f$  can be decomposed as 2-body gauge operators. Further, they can be measured by measuring the 2-body gauge operators and then combining their outputs classically even when the gauge operators in their decomposition do not commute pairwise. This is illustrated in Fig. 4. The following result was shown in Ref. [6].

**Proposition 1** (Stabilizer measurement in subsystem codes [6]). *Let  $S$  be a stabilizer of a TSCC and  $K_i$  denote a gauge generator for  $1 \leq i \leq m$ , such that  $S$  can be represented as*

$$S = K_m \cdots K_2 K_1 \quad (11)$$

where each  $K_j$  commutes with the product of all operators that appear before it, i.e.  $[K_j, K_{j-1} \cdots K_1] = 0$ ,  $j = 2, \dots, m$ . Then  $S$  can be measured by measuring the gauge operators and combining their outcomes classically.

In order to measure stabilizers using gauge operators, the decomposition specified as per Proposition 1 must be shown for all the checks which are going to be measured. The following result follows from Proposition 1. A similar result was also shown independently in [4] using a different sequence of measurements.

**Lemma 2** (Syndrome measurement of TSCC via 2-body gauge operators). *Given a TSCC, suppose that the gauge operators were measured in the following sequence:  $XX$ ,  $YY$  and  $ZZ$ . Then the stabilizers  $W_1^f$  and  $W_2^f$  of the TSCC can be reconstructed exactly from the gauge measurements.*

As mentioned earlier, the gauge generators do not commute in general. Nonetheless, the above result guarantees that it is possible to reconstruct the stabilizer measurement from the measurement outcomes of the gauge generators. Since no two  $XX$  operators overlap, they can all be measured in the same round. Similarly, all  $YY$  operators also can be measured in parallel in the same round. As to the  $ZZ$  operators, we see that for a given rank-3 edge  $(u, v, w)$ , the associated gauge operators  $Z_u Z_v$  and  $Z_v Z_w$  share a qubit. Since they commute we can measure them together. If we constrain a single qubit

to participate in only one measurement at any given time, the  $ZZ$  type operators will require two rounds of measurement. Thus two rounds are required for measuring the  $ZZ$  operators under this constraint. For the rest of the paper we will assume that all the  $ZZ$  gauge operators are measured in one round.

#### D. Mapping a TSCC onto color codes

Ref. [5] proposed a mapping of subsystem codes onto three copies of color codes. We illustrate this in Fig. 5, for the TSCC derived from the square octagon lattice. The faces of the TSCC are colored with three different colors. Qubits belonging to faces of same color are grouped together and all of them are colored the same. Each of this stack (group) of qubits can be reinterpreted as a color code, see Fig. 5. This mapping could be viewed as a reinterpretation of the operators on the subsystem code in terms of these copies of color codes.

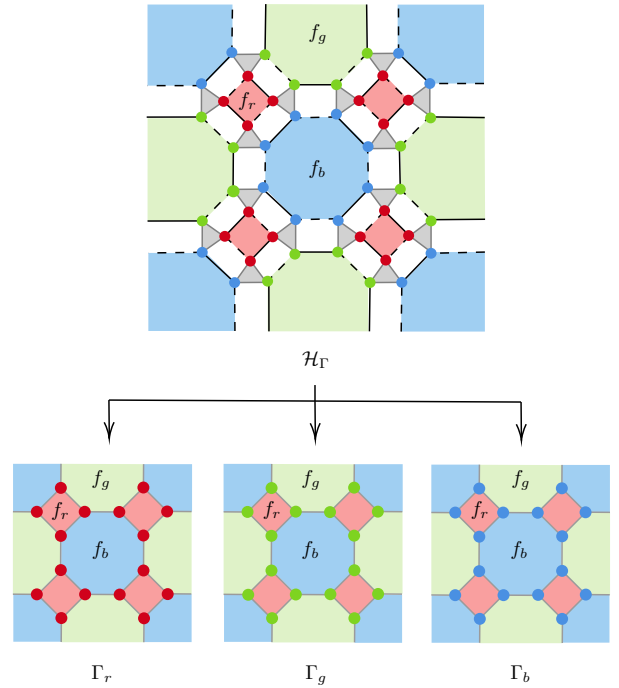


FIG. 5: Faces of TSCC are colored in red, green and blue. Qubits are highlighted with the color of the face they belong to. Every stack of qubits of same color form a color code identical to the parent color code of the TSCC. The faces in each stack are labeled same as the parent face in the hypergraph.

In mapping a TSCC to three copies of the parent TCC, we extend the stabilizer of the subsystem code to  $\mathcal{S}_e \subseteq \mathcal{G}$ , where  $\mathcal{S}_e$  is generated by all the stabilizers of the three copies of the parent color code. Therefore, we have

$$\mathcal{S} \subseteq \mathcal{G} \subseteq \mathcal{S}_e \subseteq C(\mathcal{G}) \subseteq C(\mathcal{S}_e) \subseteq C(\mathcal{S}). \quad (12)$$

Note that  $\mathcal{S}_e$  is an Abelian group. There exist other ways to map a TSCC onto color codes, see [5, 7].

### E. Error model

We assume the erasures occur independently on each qubit with a probability  $\varepsilon$ . Under the erasure model, the density matrix of a qubit ( $\rho$ ) evolves as follows:

$$\rho \longrightarrow (1 - \varepsilon)\rho + \varepsilon \frac{I}{2} \quad (13)$$

In other words, with probability  $1 - \varepsilon$ , the state remains unchanged and with probability  $\varepsilon$ , the qubit is replaced with the completely mixed state. For the purposes of decoding, we can measure the syndrome with the replaced qubit [17, 21–23]. Since the completely mixed state can be written as  $\frac{I}{2} = \frac{1}{4}\rho + \frac{1}{4}X\rho X + \frac{1}{4}Y\rho Y + \frac{1}{4}Z\rho Z$  this is equivalent to placing one of the Pauli errors,  $I, X, Y, Z$  with equal probability on the erased qubit. These errors are induced by the erasure and we refer to them as erasure induced Pauli errors. Decoding over an erasure channel requires us to correct the erasure induced Pauli errors.

## III. OVERVIEW OF THE GAUGE FIXING DECODERS

In this section we give an overview of proposed erasure decoders for TSCCs. As discussed in the previous section, for correcting the erasure errors, we can map them to Pauli errors on the erased qubits where each Pauli error occurs with equal probability. Although TSCCs are not CSS type codes, we can still correct these induced  $X$  and  $Z$  errors separately as in the case of the decoders proposed for the depolarizing channel [6, 7]. The proposed decoders have two stages: one for correcting  $X$  errors and one for correcting  $Z$  errors.

For the proposed decoders we map TSCC to three color code copies (refer Section II D) and decode over the color codes instead of decoding on the TSCC directly. Decoding by mapping onto the color codes implies that we augment the stabilizer by additional operators from the gauge group. We refer to this as gauge fixing since normally they are not constrained. However, in the proposed decoders they are also measured and treated as stabilizers. (Note that the 2-body gauge generators are not treated as stabilizers.) We propose two decoders which differ in the number of additional gauge operator, that are treated as stabilizers. Further they also differ in how the phase flip errors are corrected.

For the first decoder, bit flip errors are corrected by mapping the TSCC onto three copies of color codes. This requires additional gauge operators corresponding to the  $Z$  type stabilizers of the color codes to be measured. These are used only for correcting the bit flip errors. After the bit flip errors are corrected the phase flip errors are corrected. The  $Z$  errors are corrected using only the stabilizers of the subsystem code. The phase flip errors are corrected by mapping TSCC to the parent color code from which the subsystem color code was derived. We refer to this decoder as the *partial gauge fixing decoder*. Syndrome measurement for this decoder can be realized using 2-body measurements.

For the second decoder, the bit flip errors are corrected as in the first decoder. In addition, the phase flip errors are also

corrected by mapping them to color codes as in case of bit flip errors. This requires us to measure the gauge operators corresponding to the  $X$  type stabilizers of the color codes also. These are used for correcting the phase flip errors. The stabilizers of the subsystem code corresponding to the hypercycles are not used directly in this decoder. The total number of gauge operators that are promoted to stabilizers is almost close to the maximal set possible. We refer to this as *order maximal gauge fixing decoder*. Syndrome measurement for this decoder requires 2-body as well as 4-body measurements. However, this additional complexity leads to an improvement in performance as will be seen later.

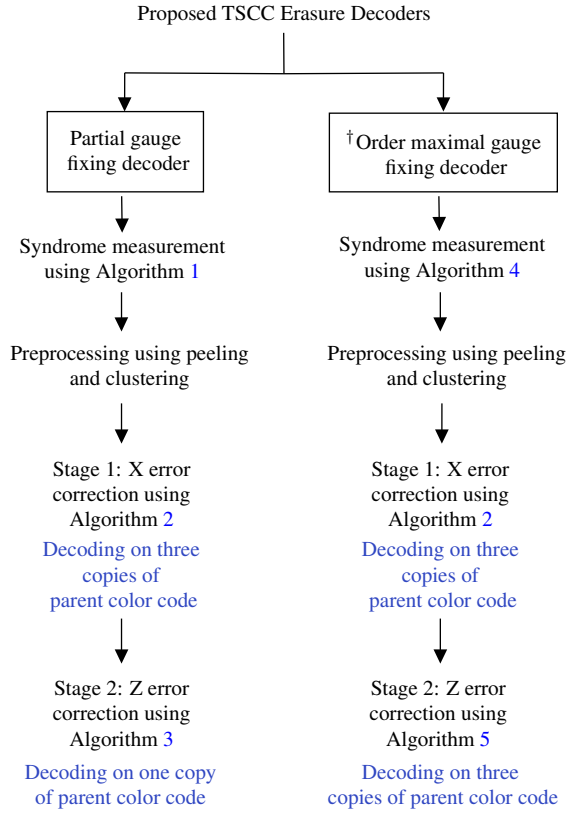


FIG. 6: Overview of proposed two stage subsystem decoders over the erasure channel.  $\dagger$ For the second decoder, the order of Stage 1 and Stage 2 can be swapped or implemented parallelly.

### A. Gauge fixing

In mapping the subsystem code to the color codes, the stabilizer of the subsystem code is extended to a larger stabilizer. This leads to gauge fixing where some of the gauge operators are promoted to checks [24]. Since our original code is a subsystem code, and we plan to decode it using the three stacks of color codes, a careful counting of the stabilizers on the color codes leads to the following observations. First of all the code we are interested in decoding is the subsystem code. This subsystem code has  $2|F|$  stabilizer generators, with two dependencies. On the other hand mapping the subsystem color

code to color code requires us to use  $2|F|$  generators for each color code i.e.  $6|F|$  stabilizer generators. (For correcting the  $X$  type errors we only need  $3|F|$  syndromes and for correcting the phase flip errors  $3|F|$ ). This means that we must be able generate additional “syndromes” on the color codes consistently. This naturally leads us to the idea of gauge fixing where in addition to the stabilizer generators of the subsystem code, we also measure some additional commuting set of gauge operators.

To obtain the additional syndromes on the color codes we could measure them directly since they commute with the stabilizer of the subsystem code. However, this would lead to losing the subsystem code advantage, namely, obtaining syndrome through 2-body measurements. We show that through an appropriate choice and sequence of gauge operators we are able to obtain the syndromes on the color codes. Furthermore, we aim to measure the color code stabilizers only through gauge measurements.

We summarize the key requirements on the measurement of syndromes for the proposed decoders in light of the above discussion on gauge fixing.

- M1. Completeness: In order that the syndromes of the color codes are generated from the gauge measurements, we also require that all their stabilizers be generated by the gauge generators. This was already known to be possible given the mappings of [5] but no proof was given therein. For completeness we give a proof of this result.
- M2. Locality: From the point of view of fault tolerance we want the decompositions of stabilizers of color codes to contain  $O(1)$  gauge operators. This is to ensure that the syndrome measurement errors can also be dealt. Every (face) stabilizer generator on color code should have a local decomposition in terms of the gauge operators on the TSCC. It is local in the sense that it involves  $O(1)$  gauge operators from that face and its neighbors.
- M3. Sequencing: The decomposition of the stabilizer generators maybe in terms of operators which are to commuting. To reconstruct the syndromes correctly, we must also provide a proper sequence in which the gauge operators are measured. This requires us to show that the sequence in which the gauge generators are measured satisfy Proposition 1 for every stabilizer generator of color codes on each stack.

There can be multiple valid sequence of measurements, but they must satisfy the above mentioned constraint so as to result in a valid syndrome. The challenge is to decide this order of measurements based on the decoding technique. We elaborate more on measurement sequences and syndrome computation in Theorem 5 and Theorem 10.

#### IV. FIRST STAGE: $X$ ERROR CORRECTION BY GAUGE FIXING

A popular approach for decoding topological codes is to map the original code into some other quantum code for which efficient decoders are known [5, 15, 25–27]. To correct the  $X$  errors we first map the TSCC onto three (identical) copies of

color codes. Each of these copies is identical to the parent color code from which the TSCC was constructed.

As shown in Fig. 5, we group the qubits into three stacks: red, green, and blue. Every stack represents a color code, and no two stacks share any common qubit. The central idea of this stage is to correct  $X$  errors on these color codes instead of directly correcting them on the TSCC. Since there is one to one correspondence between the qubits of the color codes and the TSCC, we can directly map the erasures on TSCC onto the color codes. Once the erased locations are obtained, the next step is to compute the syndrome for the  $X$  errors.

##### A. Generating syndromes on the color codes

To perform  $X$  error correction on the color codes, we need  $Z$  type stabilizer measurements. Our goal is to measure (indirectly) all the  $Z$  type stabilizers of each copy of color code via gauge measurements on TSCC. We propose a measurement map which takes measurement outcome of gauge operators from TSCC to  $Z$  type stabilizer measurement of color codes. This map must also satisfy the constraints discussed in III A.

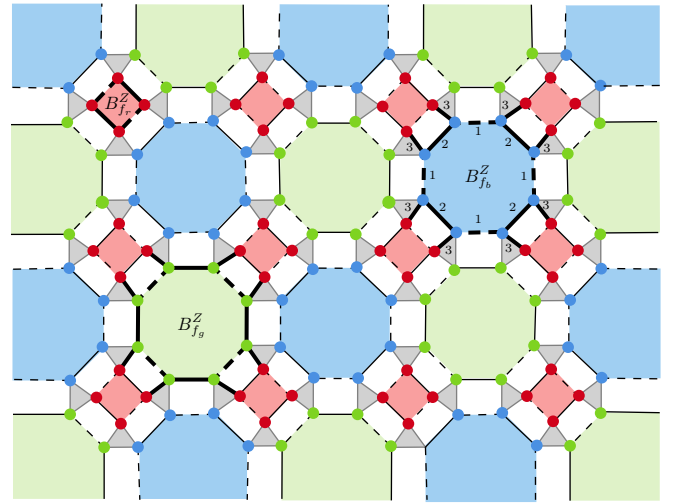


FIG. 7: Bold edges on the TSCC denote the 2-body decomposition for  $B_{f_r}^Z$ ,  $B_{f_b}^Z$  and  $B_{f_g}^Z$  stabilizers for color code on red stack. Observe that  $B_{f_r}^Z$  stabilizer on the red stack directly comes from the  $W_1^{f_r}$  TSCC stabilizer, where  $f_r$  denotes red face. Similarly,  $W_1^{f_g}$  corresponds to stabilizer  $B_{f_g}^Z$  on the green stack. With this in hand we can *push* it to the red stack by the  $ZZ$  gauge operators coming from the hyperedges. Numbers on edges of  $B_{f_b}^Z$  denote the round during which they are measured. We can check that the decompositions satisfy the conditions of Proposition 1.

Fig. 7 illustrates how the  $Z$  type stabilizers on the red stack can be measured. The figure shows which gauge operators are to be measured to obtain the  $Z$  type stabilizers on the red

stack. The bold edges marked on the TSCC depict the measured 2-body gauge operators. Similar maps can be designed for color codes on the green and blue stacks. Essentially, we obtain a decomposition of every  $Z$  type stabilizer on each of the stacks, on the TSCC, either as bare or dressed  $W_1^f$  type stabilizer, where a bare  $W_1^f$  stabilizer implies a pure rank-2 stabilizer and a dressed  $W_1^f$  stabilizer means a rank-2 stabilizer combined with some additional  $ZZ$  gauge generators.

That the stabilizer generators of the color codes can be generated by gauge generators is implicit in the mapping of the TSCC to three copies of color codes from [5]. However, explicit decompositions of the stabilizer generators of the color codes in terms of the gauge operators of the subsystem code were not given and we provide them here.

**Theorem 3** (2-body decomposition of  $Z$  type stabilizers of color codes). *Given a TSCC, every  $Z$  type stabilizer  $B_f^Z$  on each stack of the color codes can be decomposed as a product of  $O(|f|)$  gauge generators of the subsystem code.*

*Proof.* Consider the faces in  $F$ . All the stabilizers  $W_1^f$  are independent, while two of the stabilizers of type  $W_2^f$  are dependent. Each of the  $W_1^f$  type stabilizer can be mapped directly to a stabilizer on one of the stacks. More precisely,  $W_1^{f_c}$  where  $f_c \in F_c$  is mapped to the stabilizer  $B_{f_c}^Z$  on the  $c$  stack. From Eq. (4), we see that each of these stabilizers have a  $O(|f|)$  decomposition in terms of the gauge operators. This accounts for  $|F|$  stabilizers of the total  $3|F|$   $Z$  type stabilizers on all the three stacks. From the construction of the TSCC we see that every face  $f \in F$  has a rank three edge incident on each of vertices in  $f$ . Let these be denoted as  $(u_i^r, v_i^g, w_i^b)$  where  $1 \leq i \leq 2|F|$ . Each rank-3 edge  $(u_i^r, v_i^g, w_i^b)$  contains exactly one vertex from each stack. Suppose that  $u_i^r$  belongs to the red stack,  $v_i^g$  to the green stack, and  $w_i^b$  to the blue stack. Assume that  $f_g \in F_g$ . Then applying the gauge operator mentioned in Eq. (14a), the operator  $W_1^{f_g}$  can be made to act on red face, using the product  $W_1^{f_g} W_{g \rightarrow r}^{f_g}$  shown in Eq. (14b), to obtain  $(B_{f_g}^Z)_r$ , refer Eq. (14c).

$$W_{g \rightarrow r}^{f_g} = \prod_{(u_i^r, v_i^g, w_i^b) \in f_g} Z_{u_i^r} Z_{v_i^g} \quad (14a)$$

$$\begin{aligned} W_1^{f_g} W_{g \rightarrow r}^{f_g} &= W_1^{f_g} \prod_{(u_i^r, v_i^g, w_i^b) \in f_g} Z_{u_i^r} Z_{v_i^g} \\ &= \prod_{(u_i^r, v_i^g, w_i^b) \in f_g} Z_{v_i^g} \prod_{(u_i^r, v_i^g, w_i^b) \in f_g} Z_{u_i^r} Z_{v_i^g} \quad (14b) \end{aligned}$$

$$= \prod_{(u_i^r, v_i^g, w_i^b) \in f_g} Z_{u_i^r} = (B_{f_g}^Z)_r \quad (14c)$$

Observe in Eq. (14b) and Eq. (14c) how operator  $W_1^{f_g} W_{g \rightarrow r}^{f_g}$  helps us to obtain  $(B_{f_g}^Z)_r$ . We can similarly show that  $W_{b \rightarrow r}^{f_b} = \prod_i Z_{u_i^r} Z_{v_i^b}$  produces  $(B_{f_b}^Z)_r$ . In these decompositions, note that we use  $O(|f|)$  gauge generators for  $W_1^f$  and another  $O(|f|)$  gauge generators for  $W_{g \rightarrow r}^{f_g}$  giving us at most  $O(|f|)$  gauge operators in generating  $(B_{f_g}^Z)_r$ . Similarly

we need at most  $O(|f|)$  gauge operators in generating  $(B_{f_b}^Z)_r$  using  $W_{b \rightarrow r}^{f_b}$ . By a similar argument we can show that all  $Z$  type stabilizers can be measured consistently on every stack using  $O(|f|)$  gauge operators.  $\square$

**Remark 4.** Note that all the  $Z$  type stabilizer generators of the color codes on each of the three stacks are generated as elements of the gauge group of the TSCC. The dependencies among the individual color codes are respected by this decomposition. So for instance on the color code on each stack the dependencies corresponding to Eq. (5a) are also respected.

**Theorem 5** (Measurement of  $Z$  stabilizers of color codes). *Suppose that the sequence of gauge measurements is  $XX$ ,  $YY$  and  $ZZ$ . Then the stabilizers of TSCC and the  $Z$  type stabilizers of the color codes can be obtained consistently from the gauge measurements using Algorithm 1.*

*Proof.* From [6], specifically Lemma 2 we know that the stabilizer generators of the TSCC can be measured by two body gauge measurements. It remains to show that the measurement outcomes of the  $Z$  type stabilizers on the color codes can be also obtained from these two body gauge measurements. We already know that the  $Z$  type stabilizers of the TSCC can be obtained through 2-body measurements (of the gauge generators). From Eq. (14c), we see that the remaining  $Z$  type stabilizers on the color codes can also be decomposed to satisfy Proposition 1. We can use gauge operator  $W_{g \rightarrow r}^{f_g}$  to compute  $(B_{f_g}^Z)_r$  since  $W_{g \rightarrow r}^{f_g}$  commutes with  $W_1^{f_g}$ . Therefore, all  $Z$  type stabilizers of the color codes can be obtained via gauge measurements.  $\square$

Note that Algorithm 1 also returns the syndrome measurement for the stabilizers of the TSCC. These can be used to clear some simple erasure patterns using the peeling algorithm [11]. This will improve the performance of the decoders.

---

**Algorithm 1** Syndrome computation for partial gauge fixing decoder

---

**Input:** TSCC hypergraph  $\mathcal{H}_\Gamma$  and set of erasure positions  $\mathcal{E}$   
**Output:**  $X$  error syndrome  $s_c^X$  for the color code on the  $c$ -stack and syndromes of TSCC.

- 1: Measure all  $XX$  gauge generators.
- 2: Measure all  $YY$  gauge generators.
- 3: Measure all  $ZZ$  gauge generators.
- 4: Compute  $W_1^f$  stabilizer using outcomes of step 1 and 2, using the decomposition shown in Fig. 4.
- 5: Combine outcomes of step 1, 2 and 3 to get  $W_2^f$  syndrome, using the decomposition shown in Fig. 4.
- 6: **for** every  $c$ -stack,  $c \in \{r, g, b\}$  **do**
- 7:     Combine the outcomes of step 3 and 4 as per the 2-body decomposition of the color code stabilizers in Eq. (14c) to obtain the measurement of  $(B_f^Z)_c$ .
- 8: **end for**
- 9: Return  $s_c^X$ ,  $c \in \{r, g, b\}$ , measurement outcomes of  $W_1^f$  and  $W_2^f$  for all faces  $f \in F$ .

---

## B. Correcting the bit flip errors.

To correct the bit flip errors, we first map the erasures on the subsystem code to the color codes on each of the stacks. Then we measure the gauge operators in three rounds in the sequence  $XX$ ,  $YY$  and  $ZZ$ . We can then obtain the measurement outcome of  $Z$  stabilizer generators of the color codes as shown in Theorem 5. Once the syndrome on each stack is obtained, we decode the color code on that stack using a color code erasure decoder and get an error estimate. We adapt the color code erasure decoder proposed in [15]. The final step is to lift the estimate from all the color codes to the TSCC. Lifting is done in exactly reverse of how the qubits were grouped. Note that since no stack share any qubit, all the three color codes can be decoded parallelly and independently. We also update the hypercycle syndrome  $W_2^f$  at the end of this stage. The complete decoding procedure for the first stage is given in Algorithm 2.

---

### Algorithm 2 Erasure decoder stage 1: Bit flip decoder

---

**Input:** TSCC hypergraph  $\mathcal{H}_\Gamma$ , set of erasure positions  $\mathcal{E}$  and  $X$  error syndrome  $s_c^X$ .  
**Output:**  $X$  error estimate  $\hat{E}^X$

- 1:  $\hat{E}^X = I$
- 2: Group the qubits according to color of faces on TSCC.
- 3: **for** every  $c$ -stack,  $c \in \{r, g, b\}$  **do**
- 4:    $\hat{E}_c = I$
- 5:   Map erasure locations directly as per the color.
- 6:   Given  $s_c^X$ , decode color code using any color code erasure decoder to get estimate  $\hat{E}_c$ .
- 7:   Lift the estimate  $\hat{E}_c$  to the subsystem code.
- 8:   Update  $W_2^f$  syndrome according to the estimate.
- 9:   Update  $\hat{E}^X = \hat{E}^X \hat{E}_c$ .
- 10: **end for**
- 11: Return  $\hat{E}^X$  as the final  $X$  error estimate.

---

## C. Residual errors after correcting bit flip errors

As can be seen from Algorithm 2, we decode the erasure induced bit flip errors by means of a color code erasure decoder. If the decoder estimates only on the erased qubits, then we can straightaway proceed to the correction of erasure induced phase errors. However in some cases this decoder could induce some new  $Z$  type errors on the residual unerased qubits as in the case of [11], see for example Fig. 8. So this must be accounted for in the next stage. In this paper we used the erasure color code decoder proposed in [15]. This particular decoder can potentially return an error estimate on nonerased qubits up to an  $X$  type stabilizer or logical operator on the color code. (This is because the decoder works by mapping on to surface codes which can generate additional errors, see [15] for more details.) When the estimate is up to a stabilizer on the color code, on the subsystem code the error is up to an  $X$  type gauge operator because  $X$  type stabilizers on the color code are gauge operators on the subsystem code. When the estimate is up to a logical operator on the color code, on

the subsystem code the error can either be a logical operator or an  $X$  type gauge operator.

Suppose a part of the error pattern is as shown in Fig. 9a. Note that the support of the error lies only on the red color code as shown in Fig. 9b. We measure the required 2-body decompositions on the TSCC to obtain the syndrome shown in Fig. 9b. With the syndrome and erased locations, we decode the color code using color code erasure decoder and obtain error estimate as shown in Fig. 9c. Note that the estimate is not same as the original error, but it results in the same syndrome. When we apply this estimate to the original error on the color code, it results in a stabilizer as shown in Fig. 9d. (Therefore, the correction is up to a stabilizer.) When the estimate is lifted to the TSCC, we get a resultant  $X$  type gauge operator, shown in Fig. 9e. This example shows that the final outcome can induce an  $X$  type gauge error but not any additional  $Z$  errors on the unerased qubits. The following lemma proves this result formally.

**Lemma 6.** *On performing  $X$  error correction on a TSCC by decoding on three copies of color codes through Algorithm 2, the lifted error estimate can either be an  $X$  type gauge operator or a logical operator (bare or dressed). If the estimate on the color codes is up to a stabilizer, then the lifted error estimate does not contain any  $Z$  error on the unerased qubits.*

*Proof.* Suppose that the  $X$  part of the error on the TSCC is denoted  $E$  and its restriction to the color code on  $c$ -stack be  $E_c$ . Let the error estimate returned by Algorithm 2 be  $\hat{E}_c$  on the color code on the  $c$ -stack. This estimate can be decomposed as  $\hat{E}_c = E_c LS$ , where  $L$  is a logical operator and  $S$  is a stabilizer of the color code. This estimate will be a pure  $X$  type operator on the color code as it is a CSS code. When  $\hat{E}_c$  is equal to  $E$ , we get a perfect correction step and there is no residual error on the color code or the TSCC. If  $\hat{E}_c$  is not equal to  $E$ , the estimate is up to a  $X$  stabilizer or a logical operator. When this estimate is lifted to the TSCC, it can either be a logical operator or a pure  $X$  type gauge operator. If the estimate is up to a (nontrivial) logical operator on the color codes, then from Eq. (2), we see that the lifted error estimate on the subsystem code, is an  $X$  type gauge operator or a dressed logical operator of the subsystem code. Recall that a dressed logical operator is a logical operator of the TSCC augmented with additional gauge generators.

In case the estimate is up to a stabilizer on the color codes, then on the subsystem code, the estimate is up to an  $X$  type gauge operator that does not contain any  $Z$  errors on the unerased qubits. This is because the ( $X$  type) stabilizers of the color codes on each stack are in the gauge group.  $\square$

Lemma 6 shows that the lifted estimate on the TSCC does not result in any nonzero syndrome on the TSCC, therefore the second stage can also focus only on the erased qubits and ignore the unerased qubits.

Note that when the decoders on the color codes fail, it does not always lead to logical error on the TSCC as well. The following example illustrates this. Consider now the same error pattern as Fig. 8a this time decoded using Algorithm 2. For simplicity we choose an error pattern which is supported only

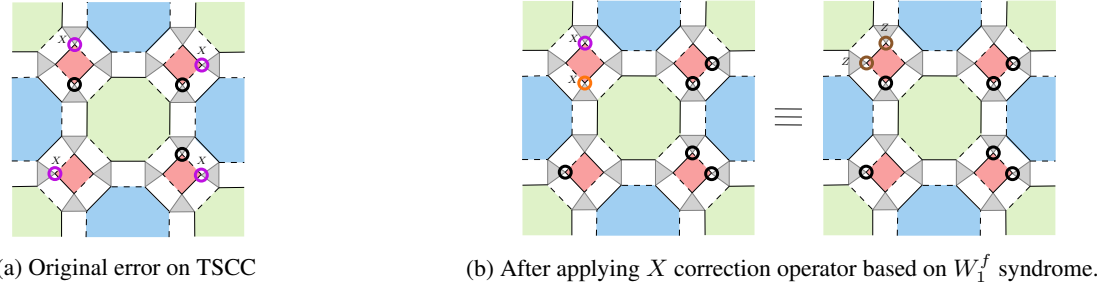


FIG. 8: Fig. 8a shows the original error on TSCC. The purple rings denote erased locations with  $X$  error and black rings denote erased locations with identity. On performing bit flip correction as per [11], the resultant TSCC is shown in Fig. 8b. The orange ring denotes the  $X$  error estimate and brown ring denotes  $Z$  error. As highlighted with green net patterned circle, there exists a residual  $Z$  error on unerased qubit as well.

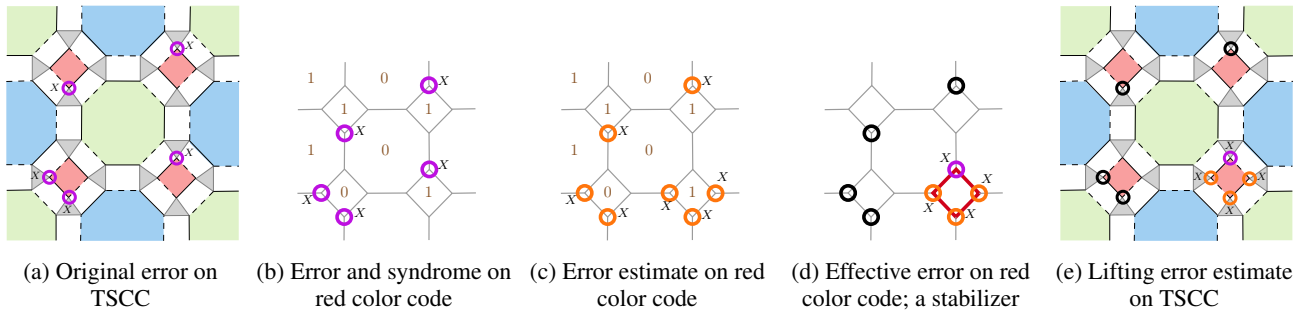


FIG. 9: Original error on TSCC is shown in Fig. 9a. Purple rings denote the erased locations with  $X$  error. Fig. 9b shows the error and syndrome on the red color code. In Fig. 9c, orange ring denote the  $X$  error estimate on red color code. Fig. 9d shows the error + error estimate on red color code. As highlighted with red, the resultant is a color code stabilizer. Fig. 9e shows how after applying the color code estimate we get resultant  $XX$  type gauge operator.

on the red faces, Fig. 10a shows the error. Fig. 10b shows the error pattern and the corresponding syndrome on the red stack. Suppose the decoder results in the estimate shown in Fig. 10c. On correcting according to this estimate, the resultant operator is a logical operator on the color code as shown in Fig. 10d. When the estimate shown in Fig. 10c is lifted to the TSCC, we get an  $X$  type gauge operator as shown in Fig. 10e. Estimate on color code up to a logical error can result to an  $X$  type gauge operator on the TSCC or a dressed logical operator on TSCC. In either case it does not create any additional  $Z$  error syndrome on the TSCC.

Parameters	Ref. [11]	Algorithm 2
Type of decoding	Local	Global
$X$ error correction on	TSCC	Three copies of color codes
Error estimate consists of	Single $X$ error	One or more $X$ errors
Error estimate	Can create residual $Z$ error on unerased qubits	Estimate is a $X$ type gauge operator or logical operator

TABLE I: Differences between first stage (bit flip error correction) of Ref. [11] decoder and proposed decoder

## V. SECOND STAGE: $Z$ ERROR CORRECTION

Before we conclude this section, in Table I we summarize the differences between the bit flip error decoding in Ref. [11] and Algorithm 2.

After performing  $X$  error correction, the next step is to correct the  $Z$  errors. In this section, we propose two algorithms to correct the  $Z$  errors. One of them uses only the stabilizers of the TSCC while the other uses additional gauge operators.

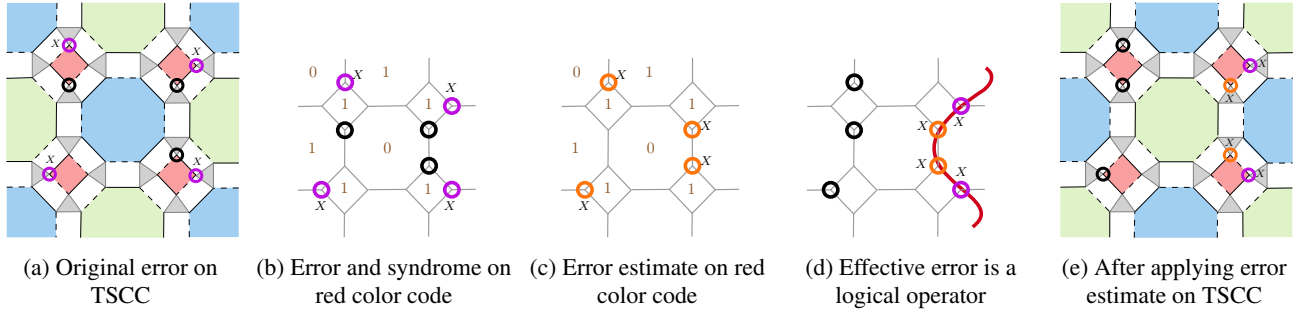


FIG. 10: The original error on TSCC is shown in Fig. 10a (same as Fig. 8a). Fig. 10b shows the error and syndrome on color code on red stack. In Fig. 10c, orange ring denote the  $X$  error estimate. Fig. 10d shows the error + error estimate on the color code. Fig. 10e shows how after applying the color code estimate we get resultant  $XX$  type gauge generators.

### A. Correcting $Z$ errors without gauge fixing

Recall that the TSCC is constructed from a 2-colex using vertex expansion. For  $Z$  error correction, we take the hypercycle syndromes of the TSCC and map them onto the parent 2-colex  $\Gamma$  from which the TSCC is derived. For face  $f$ , the hypercycle syndrome  $W_2^f$  corresponds to the  $X$  type stabilizer syndrome of the corresponding face on the 2-colex  $\Gamma$ . Since we have already cleared the  $X$  errors in the first stage, the residual syndrome on the lattice due to hypercycle stabilizers can be explained purely in terms of  $Z$  errors alone. Next we also map the erasures from the TSCC to the parent 2-colex. A vertex of the 2-colex is erased if any one or more qubits of the hyperedge (inflated triangle) in the TSCC are erased. The syndromes of the hypercycles are projected to the 2-colex. (Note that the hypercycle syndromes were updated after performing  $X$  error correction.) Once the erased locations and syndromes are obtained on the underlying color code, we can adapt any color code erasure decoder to decode it. After decoding, we lift the error estimate on the TSCC. Lifting procedure is exact reverse of how the erasures are mapped. A  $Z$  error on the color code is lifted to  $Z$  error on any one of the erased qubits on the corresponding hyperedge in the TSCC. The complete procedure for  $Z$  error correction is given in Algorithm 3.

#### Algorithm 3 Correcting $Z$ errors without gauge fixing

**Input:** TSCC hypergraph  $\mathcal{H}_\Gamma$ , set of erasure positions  $\mathcal{E}$  and syndrome of hypercycles ( $W_2^f$ ).

**Output:**  $Z$  Error estimate  $\hat{E}^Z$

- 1: Project the updated  $W_2^f$  syndromes (from Algorithm 2) to the underlying parent color code of the TSCC.
- 2: Map the erasure locations.
- 3: Adapt any color code erasure decoder to obtain an error estimate  $\tilde{E}$  (on the color code).
- 4: Lift the error estimate  $\tilde{E}$  to the TSCC. Denote the lifted estimate  $\hat{E}^Z$ .
- 5: Return  $\hat{E}^Z$  as the error estimate for  $Z$  errors.

We summarize the entire decoding algorithm. We use Algorithm 1 to compute the syndrome for decoding. We incorporate preprocessing techniques like peeling and clustering for better performance as in [11]. After performing the prepro-

cessing steps, we decode the bit flip errors using Algorithm 2, for the first stage of decoding. In the next stage we decode the phase flip errors using Algorithm 3. The complete algorithm is given in Algorithm 6. The performance of this decoder is shown in Fig. 20. We obtain a threshold of about 17.7%.

**Remark 7.** *To obtain all the measurements mentioned in Theorem 5, we measure  $3|\mathcal{F}|$   $XX$  gauge generators,  $3|\mathcal{F}|$   $YY$  gauge generators and  $4|\mathcal{F}|$   $ZZ$  gauge generators.*

**Remark 8.** *For correcting the  $X$  errors we measure, in effect,  $3|\mathcal{F}| - 6$  independent commuting operators from the gauge group and  $|\mathcal{F}| - 2$  commuting operators for correcting the  $Z$  errors. Thus a total of  $4|\mathcal{F}| - 8$  commuting gauge operators are measured. The TSCC would have measured only  $2|\mathcal{F}| - 2$  operators. Thus by partial gauge fixing we are fixing an additional  $2|\mathcal{F}| - 6$  gauge operators as checks.*

Recall from Remark 1, that the gauge group of the TSCC is generated by  $2r + s = 10|\mathcal{F}| - 2$  operators where  $s = 2|\mathcal{F}| - 2$  is the number of independent stabilizer generators of the subsystem code and  $r = 4|\mathcal{F}|$  is the number of gauge qubits. The maximal commuting subgroup in the gauge group is of size  $r + s = 6|\mathcal{F}| - 2$ . Since we measured only  $4|\mathcal{F}| - 8$  checks we see that this decoder is a partial gauge fixing algorithm.

Observe that in this decoder, the erasure induced  $X$  errors are corrected using gauge fixing while the  $Z$  errors are not. This naturally suggests the design of a decoder that fixes more gauge operators. We take this up in the next section.

### B. Correcting both $X$ and $Z$ errors with gauge fixing: Syndrome measurement and decoding procedure

In Section V A we discussed an algorithm which uses partial gauge fixing to decode TSCC. In partial gauge fixing we perform gauge fixing for clearing only bit flip errors. The phase flip errors are cleared by decoding the parent color code. The improvement in the threshold performance prompt us to fixing additional gauge generators. We now explore the correction of  $Z$  errors by gauge fixing. In partial gauge fixing, we fixed  $4|\mathcal{F}| - 8$  gauge operators out of the maximal commuting subgroup of  $6|\mathcal{F}| - 2$ . Thus an additional  $2|\mathcal{F}| - 6$  gauge operators can be fixed. In this section we correct phase flip errors

with gauge fixing, similar to bit flip error correction. We map the TSCC on to three copies of color codes and decode them for correcting phase flip errors.

To perform  $Z$  error correction on the color codes, we need to measure  $X$  type stabilizers. We need a decomposition of the  $X$  type stabilizers of the color codes in terms of the gauge generators. First, note that none of the stabilizers of the TSCC can be mapped directly to an  $X$  type stabilizer on any of the stacks. This is in contrast to the  $Z$  stabilizers of the color codes, some of which are stabilizers of the TSCC also. Thus the decompositions used for  $Z$  type stabilizers cannot be used for the  $X$  type stabilizers, refer theorem 3 for  $Z$  stabilizer decomposition. Second, the sequence of measurement of the gauge operators must be such it gives us a consistent measurement of both the  $X$  type and  $Z$  type stabilizers of the color code. This must also respect the constraints M1–M3 given in Section III A for both the  $Z$  type and  $X$  type stabilizers.

Fig. 7 shows how every  $Z$  type stabilizer of red color code can be decomposed in terms of the gauge operators of the TSCC. We show the existence of a decomposition for the  $X$  type stabilizers also. Fig. 11 shows the decomposition of the  $X$  type stabilizers of color code on red stack. (Similarly, we can also decompose the  $X$  type stabilizers of the color codes on the green and blue stacks.)

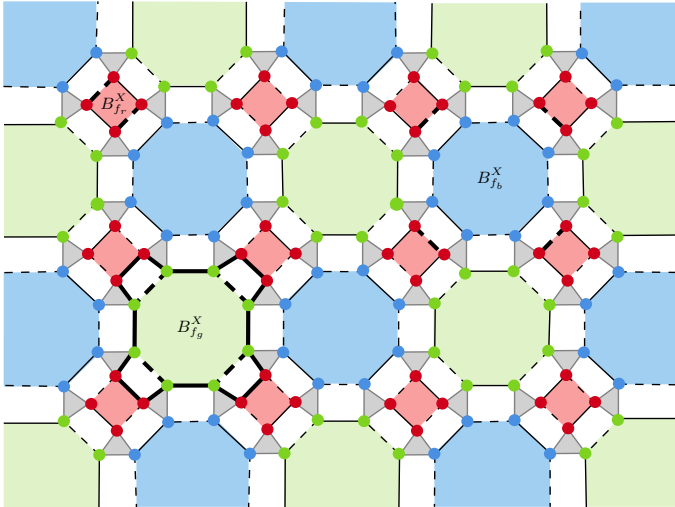


FIG. 11: Bold edges on the TSCC denote the 2-body decomposition for  $B_{f_r}^X$ ,  $B_{f_g}^X$  and  $B_{f_b}^X$  stabilizers for the color code on red stack. Observe that stabilizers  $B_{f_r}^X$  and  $B_{f_b}^X$  involve only  $XX$  type gauge generators. Decomposition of  $B_{f_g}^X$  needs all the three types of gauge generators.

The measurement of  $X$  type stabilizer generators uses the same sequence of gauge measurements assumed in Theorem 5. Notice in Fig. 11 that two types of  $X$  type stabilizers  $(B_{f_r}^X)_r$  and  $(B_{f_g}^X)_r$  are obtained using purely  $XX$  type gauge generators. Hence, after the first round of measurement (of  $XX$  gauge operators) we obtain  $X$  type stabilizers on the red and blue faces of the color code on the red stack.

In the second round we measure the  $YY$  gauge generators. This time we are able to obtain a decomposition of the  $Y$  type

stabilizers on the red and green faces on the red stack in terms of these  $YY$  gauge operators i.e.,  $(B_{f_r}^Y)_r$  and  $(B_{f_g}^Y)_r$ . These  $Y$  type stabilizers are shown in Fig. 12. In combination with the  $X$  type stabilizers on the red faces, we can also provide a decomposition of the  $Z$  type stabilizers on the red faces of the red stack. Measurements in this round allow us to compute the  $W_1^f$  stabilizers of TSCC.

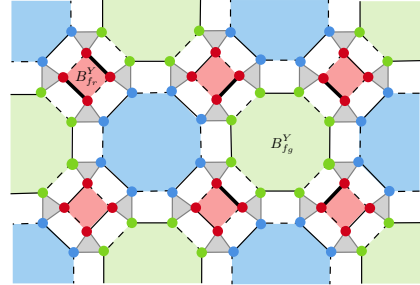


FIG. 12: Bold edges on the TSCC denote the 2-body decomposition for  $B_{f_r}^Y$  and  $B_{f_g}^Y$  stabilizers for the color code on red stack. Observe that these stabilizers consists of only  $YY$  type gauge generators. Hence these stabilizers can be obtained in the second round of gauge measurements.

For correcting  $X$  errors, we need to measure  $Z$  type stabilizers. Since we have both  $(B_{f_r}^X)_r$  and  $(B_{f_r}^Y)_r$ , we can compute the measurement outcome for  $(B_{f_r}^Z)_r$  indirectly from the measurements of  $(B_{f_r}^X)_r$  and  $(B_{f_r}^Y)_r$ .

In the third round of measurements we measure  $Z$  type gauge operators. However, measuring 2-body  $ZZ$  gauge operators will create a problem. Suppose we measure  $Z_{u_i^r}Z_{v_i^g}$ , see Fig. 13. This gauge operator will anticommute with both  $(B_{f_r}^X)_r$  and  $(B_{f_r}^Y)_r$ , if  $u_i^r \in f_r$ . On measuring this gauge operator we will no longer be in the eigenspace of  $(B_{f_r}^X)_r$  and  $(B_{f_r}^Y)_r$ . Due to this, the syndromes from the previously measured stabilizers are no longer useful. To fix this, instead of measuring a 2-body  $ZZ$  gauge generator, we directly measure a 4-body  $Z$  type gauge operator, namely  $Z_{u_i^r}Z_{v_i^g}Z_{u_j^r}Z_{v_j^g}$ , as illustrated in Fig. 13. This 4-body  $Z$  type gauge operator corresponds to the rectangle between a red face and green face. Furthermore, this 4-body operator commutes with  $(B_{f_r}^X)_r$  and  $(B_{f_r}^Y)_r$ , and therefore the previously measured syndrome values of  $(B_{f_r}^X)_r$  and  $(B_{f_r}^Y)_r$  continue to be useful for error correction.

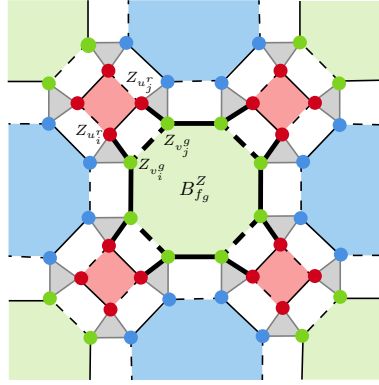


FIG. 13: Bold edges denote the gauge operators to be composed for  $B_{f_g}^Z$  stabilizer for color code on red stack. The highlighted 4-body  $Z$  type gauge operators are to be measured to compute the syndrome. When sequence of measurement is  $XX$  type gauge operators first,  $YY$  type gauge operators second and  $U_f^\square$  type gauge operators last, this decomposition satisfies Proposition 1.

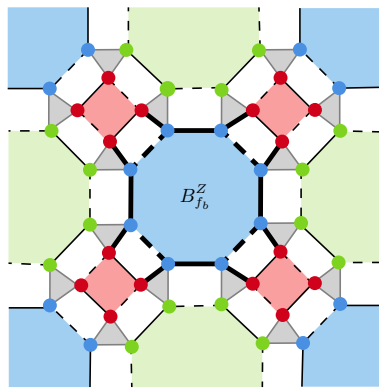


FIG. 14: Bold edges denote the gauge operators to be composed for  $B_{f_b}^Z$  stabilizer for color code on red stack. The highlighted 4-body  $Z$  type gauge operators are to be measured to compute the syndrome. When sequence of measurement is  $XX$  type gauge operators first,  $YY$  type gauge operators second and  $U_f^\square$  type gauge operators last, this decomposition satisfies Proposition 1.

For every rectangular face  $f \in \mathcal{F}_4$  we define a  $Z$  type gauge operator  $U_f^\square$  acting on every vertex of  $f$ . More precisely, we have

$$U_f^\square = \prod_{i \in f} Z_i \quad (15)$$

Note that  $U_f^\square$  is a 4-body operator since there are four vertices for every rectangle face. Furthermore,  $U_f^\square$  commutes with all the stabilizer generators of the color codes on all the stacks and  $U_f^\square$  commutes with  $U_{f'}^\square$  for all  $f' \in \mathcal{F}_4$ . Let  $N(f)$  be the set of rectangles sharing a rank-2 edge with face  $f \in \mathcal{F}$ .

Consider the following gauge operator

$$V_{g \rightarrow r}^{f_g} = \prod_{f \in N(f_g) \cap \mathcal{F}_{rg}} U_f^\square \quad (16)$$

Then using  $V_{g \rightarrow r}^{f_g}$  we can obtain  $(B_{f_g}^Z)_r$  from  $W_1^{f_g}$  as follows.

$$(B_{f_g}^Z)_r = V_{g \rightarrow r}^{f_g} W_1^{f_g} \quad (17)$$

Note that the above decomposition for  $(B_{f_g}^Z)_r$  satisfies Proposition 1 and therefore it can be measured consistently from the gauge operators forming the decomposition. We can also obtain  $(B_{f_b}^Z)_r$  stabilizer in the same way.

Since we have already obtained  $(B_{f_g}^Y)_r$  in the second round of measurement, we combine  $(B_{f_g}^Y)_r$  and  $(B_{f_g}^Z)_r$  to obtain  $(B_{f_g}^X)_r$  indirectly, see Fig. 15. This shows how the stabilizers of the color code on the red stack can be measured by measuring 2-body gauge operators of  $X$  and  $Y$  type and 4-body  $Z$  type gauge operators.

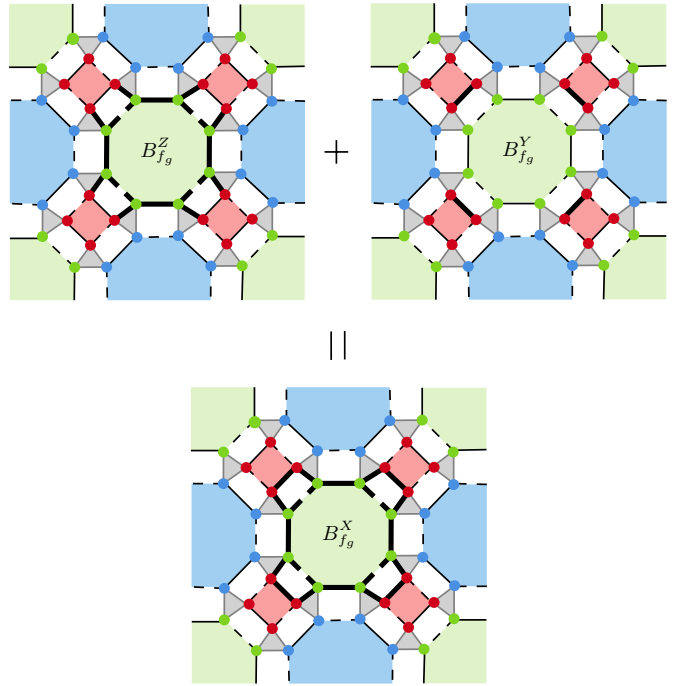


FIG. 15: Generating syndrome for stabilizer  $(B_{f_g}^X)_r$  by summing syndromes of  $(B_{f_g}^Z)_r$  and  $(B_{f_g}^Y)_r$ .

The following theorem summarizes the preceding discussion about the decomposition of all stabilizers on the three copies of the color codes.

**Theorem 9** (2-body and 4-body decomposition of  $X$  type and  $Z$  type stabilizers of color codes). *Given a TSCC, every  $X$  type stabilizer and  $Z$  type stabilizer on each stack of the color codes can be decomposed as a product of  $O(|f|)$  gauge operators of the subsystem code. The  $Z$  type gauge operators are 4-body measurements while the  $XX$  and  $YY$  gauge operators are 2-body measurements.*

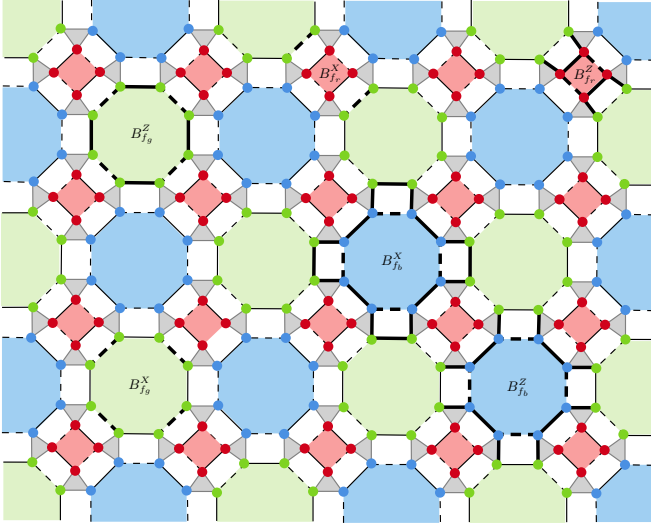


FIG. 16:  $X$  type and  $Z$  type Stabilizers for color code on green stack.

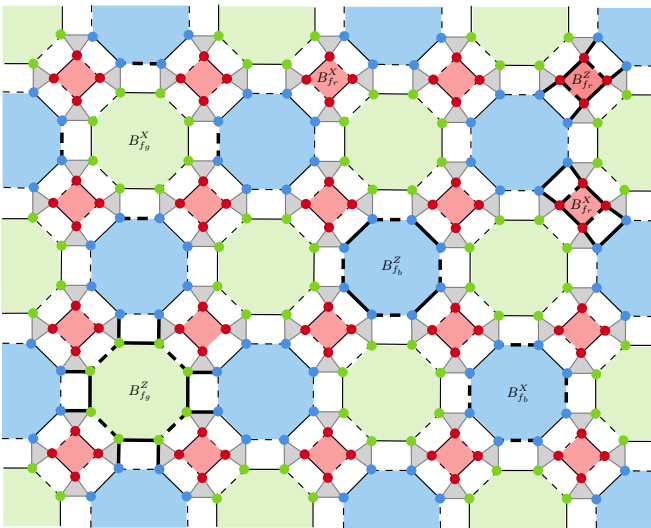


FIG. 17:  $X$  type and  $Z$  type Stabilizers for color code on blue stack.

While Theorem 9 shows that the stabilizers of the color codes can be decomposed in terms of the gauge generators, it does not show that these commuting set of operators can be measured simultaneously with 2-body operators. We give a sequence of measurement of the gauge operators involving at most 4-body operators such that all the stabilizers of the color codes can be measured simultaneously.

**Theorem 10** (Measurement of  $X$  and  $Z$  stabilizers of color codes). *Suppose that the sequence of measurements of the gauge operators is as follows:*

- i) 2-body  $XX$  gauge generators
- ii) 2-body  $YY$  gauge generators
- iii) 4-body  $ZZ$  gauge operator of the form  $U_f^\square$  where  $f \in \mathcal{F}_4$ . Then all  $X$  type and  $Z$  type stabilizers of the color codes and

the stabilizers of the TSCC can be obtained consistently from these gauge measurements using Algorithm 4.

*Proof.* After measuring the  $XX$  type gauge operators we can obtain the  $X$  type stabilizers for  $f \in \mathcal{F}_c$  for the color code on the  $c$  stack, see Fig. 11 for  $B_{f_r}^X$  stabilizer of color code on red stack. In addition for each of the stacks we also obtain the  $X$  type stabilizers for the faces on another color  $c'$ . For the red stack, we also obtain  $B_f^X$  for  $f \in \mathcal{F}_b$ , for the blue stack we obtain  $B_f^X$  for  $f \in \mathcal{F}_g$  and for the green stack we also obtain  $B_f^X$  for  $f \in \mathcal{F}_r$ . Table II shows the stabilizers obtained after every round of measurement. Entries marked with 1 are the stabilizers which are measured after the first round of measurement.

This leaves the  $X$  type stabilizers on  $f \in \mathcal{F}_g$  for the red stack,  $f \in \mathcal{F}_r$  for the blue stack and  $f \in \mathcal{F}_b$  for the green stack. To measure these stabilizers via the gauge measurements, we must first measure the  $YY$  type gauge operators followed by the 4-body  $Z$  type operators  $U_f^\square$ .

On measuring the  $YY$  type gauge operators, we can immediately see that they also can be used to measure the  $B_f^Y$  for  $f \in \mathcal{F}_c$  on the  $c$  stack, refer Fig. 12. The  $YY$  gauge operators are disjoint and can be seen to easily satisfy Proposition 1. Furthermore, they also commutes with the previously measured  $X$  type stabilizers in the first round. On the red stack these  $YY$  gauge operators also allow us to measure the  $(B_{f_g}^Y)_r$  for  $f \in \mathcal{F}_g$ . Similarly, the  $YY$  gauge operators also give  $B_{f_g}^Y$  and  $B_{f_b}^Y$  stabilizers on green stack and  $B_{f_r}^Y$  and  $B_{f_b}^Y$  stabilizers on blue stack.

From Table II, we see that on the red stack both  $(B_{f_r}^X)_r$  and  $(B_{f_r}^Y)_r$  are available for all the faces  $f_r \in \mathcal{F}_r$  allowing us to obtain  $(B_{f_r}^Z)_r$ . Likewise we can also obtain  $B_{f_g}^Z$  on green stack and  $B_{f_b}^Z$  on blue stack. However, the remaining  $Z$  type stabilizers on the other faces are not yet measured.

At this point we do not have the measurement outcomes for  $(B_f^Y)$  on i) the blue faces of the red stack, ii) red faces of the green stack and iii) green faces on the blue stack, refer Table II.

In the third round, we measure the 4-body gauge operators  $U_f^\square$  for  $f \in \mathcal{F}_4$ . Observe the decomposition given in Fig. 13 satisfies the conditions in Proposition 1. Therefore, for the color code on the red stack, we can measure  $(B_{f_g}^Z)_r$  for all  $f_g \in \mathcal{F}_r$ . Similarly, using the decomposition given in Fig. 14, we can measure  $(B_{f_b}^Z)_r$  for all  $f_b \in \mathcal{F}_b$ .

At this point, we have all the  $X$  type stabilizers on the red stack and therefore can correct all the bit flip errors. For decoding the  $Z$ , we need the  $X$  type stabilizers but the stabilizers  $B_{f_g}^X$  are missing. These can be obtained from  $(B_{f_g}^Y)_r$  and  $(B_{f_g}^Z)_r$  which we already have.

Using the symmetry of the color code with respect to the colors, we can therefore conclude that all the stabilizers on each of the stacks can be obtained by the given sequence of measurements and using the decomposition given in Fig. 16 and 17.

Stabilizer	Color code on red stack	Color code on green stack	Color code on blue stack
$B_{f_r}^X$	1 Fig. 11	1	$3$ $(B_{f_r}^Z)_b + (B_{f_r}^Y)_b$
$B_{f_g}^X$	$3$ $(B_{f_g}^Z)_r + (B_{f_g}^Y)_r$	1	1
$B_{f_b}^X$	1 Fig. 11	$3$ $(B_{f_b}^Z)_g + (B_{f_b}^Y)_g$	1
$B_{f_r}^Y$	2 Fig. 12	$3$ $(B_{f_r}^X)_g + (B_{f_r}^Z)_g$	2
$B_{f_g}^Y$	2 Fig. 12	2	$3$ $(B_{f_g}^X)_b + (B_{f_g}^Z)_b$
$B_{f_b}^Y$	$3$ $(B_{f_b}^X)_r + (B_{f_b}^Z)_r$	2	2
$B_{f_r}^Z$	$2$ $(B_{f_r}^X)_r + (B_{f_r}^Y)_r$	3	3
$B_{f_g}^Z$	$3$ Fig. 13	$2$ $(B_{f_g}^X)_g + (B_{f_g}^Y)_g$	3
$B_{f_b}^Z$	$3$ Fig. 14	3	$2$ $(B_{f_b}^X)_b + (B_{f_b}^Y)_b$

TABLE II: Color code stabilizers obtained at the end of every round of measurement. The number denotes the measurement round. Here  $f_c$  indicates that the face is of color  $c$ . The decompositions for the stabilizers on the green and blue stacks are given Fig. 16 and 17 respectively. The measurements of the shaded ones are obtained indirectly. For instance,  $B_{f_g}^X$  is obtained after the measurement of  $B_{f_g}^Z$  and  $B_{f_g}^Y$ .

Recall that each of the stabilizer  $W_1^f$  corresponds to a stabilizer on the color code. Therefore, it follows that all stabilizers can be obtained. On the other hand, none of the hypercycle stabilizers  $W_2^f$  corresponds to a stabilizer on any stack since they have support on all three stacks. However, the hypercycle stabilizer  $W_2^f$  can be decomposed into three stabilizers each supported on a stack of different color, see Fig. 18. The figure shows how  $X$  type stabilizer on the red stack and  $Y$  type stabilizers on the blue and green stacks can be combined to form the hypercycle stabilizer on green face of TSCC.

$$W_2^{f_r} = (B_{f_r}^Y)_r (B_{f_r}^Y)_g (B_{f_r}^X)_b \quad (18a)$$

$$W_2^{f_g} = (B_{f_g}^X)_r (B_{f_g}^Y)_g (B_{f_g}^Y)_b \quad (18b)$$

$$W_2^{f_b} = (B_{f_b}^Y)_r (B_{f_b}^X)_g (B_{f_b}^Y)_b \quad (18c)$$

Using these decompositions, we can also measure the syndromes of the TSCCs using the given sequence of measurement of the gauge operators. Algorithm 4 describes how the syndrome measurement takes place for both  $X$  and  $Z$  type color code stabilizers and TSCC stabilizers.  $\square$

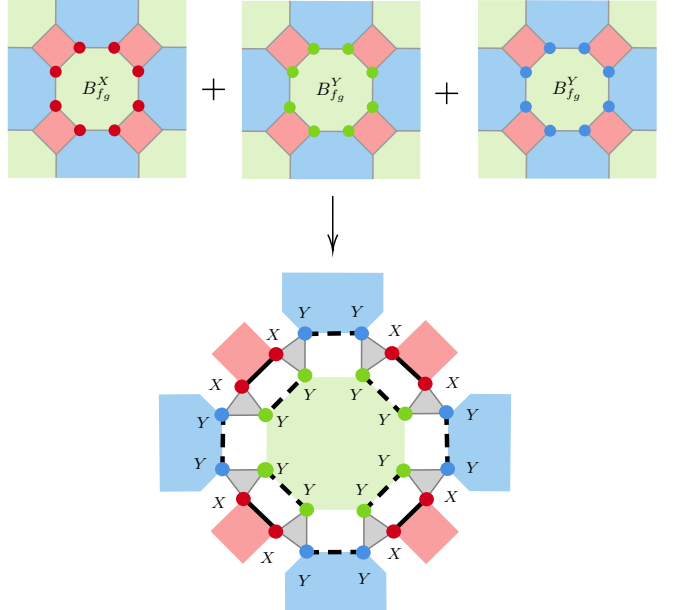


FIG. 18: Decomposition of  $W_2^{f_g}$  into the stabilizers on color codes, namely,  $(B_{f_g}^X)_r$ ,  $(B_{f_g}^Y)_g$ , and  $(B_{f_g}^Y)_b$ .

---

**Algorithm 4** Syndrome computation for order maximal gauge fixing.

---

**Input:** TSCC hypergraph  $\mathcal{H}_\Gamma$  and set of erasure positions  $\mathcal{E}$   
**Output:**  $X$  error syndrome  $s_c^X$  and  $Z$  error syndrome  $s_c^Z$  for the color code on the  $c$ -stack and syndrome of TSCC.

- 1: Measure all 2-body  $XX$  gauge generators.
- 2: Compute color code stabilizers with entries ‘1’ in Table II.
- 3: Measure all 2-body  $YY$  gauge generators.
- 4: Compute color code stabilizers with entries ‘2’ in Table II.
- 5: Measure all 4-body  $ZZZZ$  gauge operators for face  $f \in \mathcal{F}_4$ .
- 6: Compute color code stabilizers with entries ‘3’ in Table II.
- 7: Calculate  $W_2^f$  using Eq. (18) for all  $f \in \mathcal{F}$ .
- 8: Return  $s_c^Z$  and  $s_c^X$ ,  $c \in \{r, g, b\}$ , syndromes of  $W_1^f$  and  $W_2^f$ .  $\triangleright$   
 $W_1^f$  includes  $B_{f_c}^Z$  stabilizer of  $c$ -stack.

---

**Remark 11.** To obtain all the measurements mentioned in Theorem 10, we measure  $3|\mathcal{F}|$   $XX$  gauge generators,  $3|\mathcal{F}|$   $YY$  gauge generators and  $3|\mathcal{F}|$   $ZZZZ$  gauge generators.

**Remark 12.** From the proof of Theorem 10, we can see that in effect we are measuring  $6|\mathcal{F}| - 12$  independent stabilizers. Thus compared to the TSCC where we measure  $2|\mathcal{F}| - 2$  stabilizers we are measuring in addition  $4|\mathcal{F}| - 10$  gauge operators. On TSCC it is possible to gauge fix at most  $r+s = 6|\mathcal{F}| - 2$  stabilizers, thus we are order maximal with respect to the number of gauge operators that are being fixed.

**Remark 13.** If we are constrained to have one qubit to participate only in one measurement at a time, then measurement of the 4-body  $Z$  type operators i.e.,  $U_f^\square$  will require three rounds. In one round, we measure all  $U_f^\square$  where  $f \in \mathcal{F}_{cc'}$  and  $cc' \in \{rg, rb, bg\}$ . Under this constraint, we have total five rounds of measurements: one round for  $XX$  type opera-

tors, one round for  $YY$  type operators and three rounds for  $ZZZZ$  type operators.

For decoding the TSCC we can use the stabilizers of the color codes and proceed to decode independently on each of the stacks. Since Theorem 10 shows that we can also measure the TSCC stabilizers along with the stabilizers of the color codes, we use them to preprocess the erasures before decoding on the color codes. We were motivated by the fact that preprocessing using peeling led to an improvement in the performance [11].

We obtain syndromes for  $X$  type stabilizers of the color codes as discussed in Theorem 10. Once the color code syndromes are obtained, we decode the color codes by adapting a color code erasure decoder. We then lift the joint estimate on all the stacks back to the TSCC. We lift the error estimate back on the TSCC according to the color of the color code. Since color code is a CSS code, we can perform  $X$  error correction and  $Z$  error correction in any order. Considering we clear both  $X$  and  $Z$  error on the copies of color codes, we perform gauge fixing for correcting both the errors. Algorithm 5 describes the decoding procedure for phase flip errors with gauge fixing.

---

**Algorithm 5** Correcting  $Z$  errors with gauge fixing

---

**Input:** TSCC hypergraph  $\mathcal{H}_\Gamma$  and set of erasure positions  $\mathcal{E}$

**Output:**  $Z$  Error estimate  $\hat{E}^Z$

- 1:  $\hat{E}^Z = I$
- 2: Group the qubits according to color of faces on TSCC.
- 3: **for** every  $c$ -stack,  $c \in \{r, g, b\}$  **do**
- 4:    $\hat{E}_c = I$
- 5:   Map erasure locations directly as per the color.
- 6:   Obtain syndrome  $s_c^X$  using Algorithm 4.
- 7:   Decode color code by adapting any color code erasure decoder to get estimate  $\hat{E}_c$ .
- 8:   Lift the estimate  $\hat{E}_c$  to the subsystem code.
- 9:   Update  $W_2^f$  syndrome according to the estimate.
- 10:   Update  $\hat{E}^Z = \hat{E}^Z \hat{E}_c$ .
- 11: **end for**
- 12: Return  $\hat{E}^Z$  as the final  $Z$  error estimate.

---

From Eq. (18), we have that the hypercycle stabilizer of TSCC can be decomposed to a sum of color code stabilizers. Therefore, clearing the syndromes on the color codes also clears the syndrome on the TSCC. This makes sure that correction restores the state to the codespace, namely, the joint  $+1$ -eigenspace of the subsystem code stabilizers.

### C. Complete algorithm

In this section we summarize both the  $X$  and  $Z$  correction for both approaches. The complete algorithm is given in Algorithm 6. The first step is to obtain the necessary syndromes for decoding the TSCC. If we are decoding with the partial gauge fixing decoder, we use Algorithm 1. For order maximal gauge fixing, we use Algorithm 4.

Along with the syndromes of the color codes, we also compute the syndrome of the TSCC which helps in the preprocessing, namely peeling, refer Algorithm 2 in [11].

The second step is to preprocess using peeling. During peeling we correct single isolated erasures using TSCC stabilizer measurements. Peeling results in removal of erasures and also updates syndromes of some of the stabilizers of the TSCC and the color codes. Based on the location of the erasure where the correction is applied, we modify the color code syndromes as per the stack it belongs to. An erased qubit belonging to a face  $f_c$  of TSCC modifies only syndromes of color code on  $c$ -stack. We also update the hypercycle stabilizer syndromes. They are used for phase flip error correction during partial gauge fixing decoding. We do not need to keep track of the hypercycle syndromes for the order maximal gauge fixing decoder since we do not utilize them for further error correction.

After peeling, some of the erasures are corrected and the syndromes appropriately modified. Peeling is followed by clustering of erasures. We scan the lattice from left to right and top to bottom and search for a stabilizer which contains at least one erased qubit. We group the erased qubits of the stabilizer to form a cluster. (This is true even if there is a single erasure in that stabilizer.) For each of the erased qubit we check if it is already part of a previously formed cluster. If so, we merge these clusters. For more details, see [11]. We repeat this procedure for every stabilizer. At the end, erasures of two distinct clusters do not participate in a common stabilizer.

Once the clusters are formed, the next step is to decode every cluster independently. For every cluster, we perform bit flip error correction using Algorithm 2. We then correct the phase flip errors. If decoding with partial gauge fixing decoder, we use Algorithm 3 and for order maximal gauge fixing decoder, we use Algorithm 5. All error estimates for each of the clusters are combined and returned at the end of the algorithm.

**Algorithm 6** Erasure decoder for TSCC

---

**Input:** TSCC hypergraph  $\mathcal{H}_\Gamma$ , set of erasure positions  $\mathcal{E}$  and choice of decoding: partial gauge fixing decoding or order maximal gauge fixing decoding.

**Output:** Error estimate  $\hat{E}$

- 1:  $\hat{E} = I$ .
- 2: **if** partial gauge fixing decoding **then**
- 3:   Use Algorithm 1 to obtain syndrome  $s_c^X$ ,  $c \in \{r, g, b\}$  and syndromes of  $W_1^f$  and  $W_2^f$  for all  $f \in \mathcal{F}$ .
- 4: **else**
- 5:   Use Algorithm 4 to obtain syndrome  $s_c^X$  and  $s_c^Y$ ,  $c \in \{r, g, b\}$  and syndromes of  $W_1^f$  and  $W_2^f$  for all  $f \in \mathcal{F}$ .
- 6: **end if**
- 7: Perform peeling to obtain correction operator  $\hat{E}_p$ , refer [11].
- 8: Update the color code and TSCC stabilizers and the list of erasures.
- 9: Cluster remaining erasures which share a stabilizer.  $\triangleright$  Let the number of clusters be  $n_c$
- 10: **if**  $1 \leq i \leq n_c$  **then**
- 11:   Use Algorithm 2 to obtain  $X$  error estimate  $\hat{E}^X$ .
- 12:   **if** partial gauge fixing decoder **then**
- 13:     Use Algorithm 3 to obtain  $Z$  error estimate  $\hat{E}^Z$ .
- 14:   **else**
- 15:     Use Algorithm 5 to obtain  $Z$  error estimate  $\hat{E}^Z$ .
- 16:   **end if**
- 17:    $\hat{E} = \hat{E}\hat{E}^X\hat{E}^Z$
- 18: **end if**
- 19: Return  $\hat{E}\hat{E}_p$  as the final error estimate.

---

We obtained a threshold of 44% for the order maximal gauge fixing decoder, shown in Fig. 21. In Table III we highlight the key differences between the decoders. Note that for order maximal gauge fixing since both bit flip error syndrome and phase flip error syndrome do not affect each other, we can decode both these errors in parallel. We discuss the simulation results in Section VII. Before that, we study the correctability of erasure patterns on TSCCs in the next section.

## VI. CORRECTABILITY CONDITION ON ERASURE PATTERN

In this section we propose correctability conditions for an erasure pattern on subsystem codes. Using the correctability condition we can test, prior to decoding, whether an erasure pattern can be corrected or not. In Theorem 14, we propose the condition for a general subsystem code.

Before we begin, we introduce a few notations necessary for this section. We denote the stabilizer matrix of the subsystem code by  $H$  and matrix representation of the gauge group over  $\mathbb{F}_2$  by  $G$ . The stabilizer matrix  $H$  involves all the (independent) stabilizer generators of the subsystem code while  $G$  consists of the gauge generators. Let  $H_{\mathcal{E}}$  be a submatrix which is a restriction of  $H$  to the subset of columns corresponding to locations of erased qubits. Similarly, we denote by  $G_{\mathcal{E}}$  and  $G_{\bar{\mathcal{E}}}$ , the submatrices of  $G$  restricted to the qubits in  $\mathcal{E}$  and  $\bar{\mathcal{E}}$  respectively. The submatrix  $H_{\bar{\mathcal{E}}}$  consists of the remaining columns of  $H$ . We denote the stabilizer matrix of the parent color code by  $H_c$ , where  $c \in \{r, g, b\}$ .

An erasure pattern  $\mathcal{E}$  is correctable if all the errors supported in  $\mathcal{E}$  are correctable and non-correctable otherwise. Equivalently, if  $\mathcal{E}$  supports a logical error, then it is not correctable and correctable otherwise. A necessary condition for an erasure pattern to be correctable for stabilizer codes due to [23] is as follows:

**Proposition 2** ([23]). *For stabilizer codes, an erasure pattern  $\mathcal{E}$  is correctable only if*

$$2|\mathcal{E}| \leq \text{rank}(H) + \text{rank}(H_{\mathcal{E}}) - \text{rank}(H_{\bar{\mathcal{E}}}) \quad (19)$$

*Proposition 2 immediately gives a sufficient condition for a correctable erasure pattern decoded via order maximal gauge fixing decoder. Specifically, if Eq. (19) is satisfied on all the three copies of color code i.e.,*

$$2|\mathcal{E}_c| \leq \text{rank}(H_c) + \text{rank}(H_{\mathcal{E}_c}) - \text{rank}(H_{\bar{\mathcal{E}}_c}) \quad (20)$$

for every  $c$ , where  $c \in \{r, g, b\}$ , then the erasure is correctable by the order maximal gauge fixing decoder. Note that this is only a sufficient condition for the correctability of an erasure pattern and not a necessary condition, see the discussion in Section IV C.

We now propose a condition for correctable erasures applicable to general subsystem codes decoded without gauge fixing. This condition also accounts for the gauge group.

**Theorem 14** (Correctable erasures on a TSCC without gauge fixing). *An erasure pattern  $\mathcal{E}$  on a TSCC is correctable only if the following condition is satisfied.*

$$2|\mathcal{E}| = \text{rank}(H_{\mathcal{E}}) + \text{rank}(G) - \text{rank}(G_{\bar{\mathcal{E}}}) \quad (21)$$

*Proof.* Up to a phase, there are  $4^{|\mathcal{E}|}$  Pauli errors that can be supported in  $\mathcal{E}$ . There are  $2^{\text{rank}(H_{\mathcal{E}})}$  syndromes possible. For each syndrome there exist  $2^{2|\mathcal{E}| - \text{rank}(H_{\mathcal{E}})}$  error patterns. Consider the map

$$\pi_{\bar{\mathcal{E}}} : G \rightarrow G_{\bar{\mathcal{E}}} \quad (22)$$

The operators in the kernel of  $\pi_{\bar{\mathcal{E}}}$  are exactly the operators in  $G$  whose support is entirely in  $\mathcal{E}$ . The dimension of  $\ker \pi_{\bar{\mathcal{E}}}$  is given by

$$\ker(\pi_{\bar{\mathcal{E}}}) = \text{rank}(G) - \text{rank}(G_{\bar{\mathcal{E}}}) \quad (23)$$

All errors in  $\ker(\pi_{\bar{\mathcal{E}}})$  have support only in  $\mathcal{E}$  and have zero syndrome. First observe that such errors cannot be more than the total number of errors supported in  $\mathcal{E}$  which have zero syndrome. Therefore,  $\text{rank}(G) - \text{rank}(G_{\bar{\mathcal{E}}}) \leq 2|\mathcal{E}| - \text{rank}(H_{\mathcal{E}})$ . If errors in  $\ker(\pi_{\bar{\mathcal{E}}})$  are fewer than the number of distinct errors with the same syndrome, then  $\mathcal{E}$  supports nontrivial logical error(s). Therefore, if  $\text{rank}(G) - \text{rank}(G_{\bar{\mathcal{E}}}) < 2|\mathcal{E}| - \text{rank}(H_{\mathcal{E}})$ , then  $\mathcal{E}$  is not correctable. If  $2|\mathcal{E}| - \text{rank}(H_{\mathcal{E}}) = \text{rank}(G) - \text{rank}(G_{\bar{\mathcal{E}}})$ , all such errors are in the gauge group. So  $\mathcal{E}$  does not support a (nontrivial) logical operator and  $\mathcal{E}$  is a correctable erasure pattern.  $\square$

**Remark 15.** *Since it is not possible for  $\text{rank}(G) - \text{rank}(G_{\bar{\mathcal{E}}}) > 2|\mathcal{E}| - \text{rank}(H_{\mathcal{E}})$ , we can state the correctability*

Decoder	Partial gauge fixing decoder	Maximal gauge fixing decoder
Lattice for $X$ error correction	Three copies of (parent) color code of the TSCC.	
$X$ error correction	Map erasures and syndrome to three copies of color codes. Decode them using an erasure decoder.	
Lattice for $Z$ error correction	Parent color code of TSCC	Three copies of (parent) color code
$Z$ error correction	Map $W_2^f$ syndrome and erased locations to the parent color code. Decode using an erasure decoder	Map erasures and syndrome to three copies of color codes. Decode them using an erasure decoder.
Number of commuting gauge operators to be measured	$4 \mathcal{F}  - 8$	$6 \mathcal{F}  - 12$
Number of times color code erasure decoder is utilized	4	6
Errors for which gauge fixing is used	Only $X$ errors	Both $X$ and $Z$ errors
Number of gauge operators measured	$XX$	$3 \mathcal{F} $
	$YY$	$3 \mathcal{F} $
	$ZZ$	$4 \mathcal{F} $
	$ZZZZ$	0
Threshold	17.7%	44%

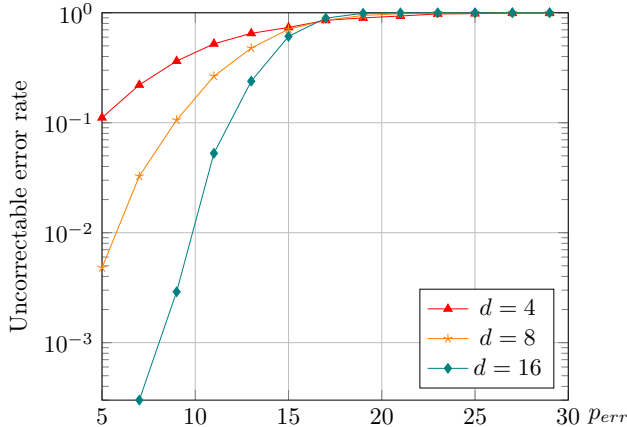
TABLE III: Comparison between partial gauge fixing decoder and order maximal gauge fixing decoder.

condition in Theorem 14 slightly differently. More precisely, an erasure is correctable only if

$$2|\mathcal{E}| \leq \text{rank}(H_{\mathcal{E}}) + \text{rank}(G) - \text{rank}(G_{\bar{\mathcal{E}}}) \quad (24)$$

In this form it reduces to the condition in [23, Eq. (4)], when  $G$  is Abelian i.e., we have a stabilizer code.

We performed simulations based on the condition in Eq. (21). We generate an erasure pattern  $\mathcal{E}$  where qubit is erased with a probability  $\varepsilon$  on the subsystem code. As per the locations of  $\mathcal{E}$ , we compute the rank of the matrices  $H_{\mathcal{E}}$  and  $G_{\bar{\mathcal{E}}}$ . Rank of  $G$  remains constant throughout the simulations since it is independent of  $\mathcal{E}$ . If the condition in Eq. (21) gets violated, we flag it as an uncorrectable error. We repeated the experiment for 10000 trials for various  $\varepsilon$  for code distances  $d = 4, 8, 16$ . We obtained a threshold of approximately 16.5% as shown in Fig. 19.

FIG. 19: Threshold of  $\approx 16.5\%$  based on Eq. (21).

## VII. SIMULATION RESULTS

In this section we present the simulation results for both the decoding algorithms. We simulate for the TSCC derived from square octagon lattice. The proposed algorithms can be easily adapted to other TSCCs.

### A. Simulation setup

An erasure pattern is generated on the subsystem codes according to the probability of erasure  $\varepsilon$ . Noise on each qubit is assumed to be identical and independent. Then using the erasure model described in Section II E, we generate Pauli errors on each of the erased qubits with equal probability. Every erased location can undergo any of the Pauli errors with equal probability as described in Section II E. Then we correct these induced Pauli errors on the subsystem code. We use Algorithm 6 for decoding.

In practice, while decoding a subsystem code, its stabilizers are measured indirectly via measuring the gauge generators and classically combining the outcomes appropriately. The proposed decoders map the TSCCs to multiple copies of color codes in order to decode them. Theorem 5 and Theorem 10 show how to obtain measurement outcomes for the color code stabilizers by measuring the gauge operators. For simulation purposes, we measured the multi-body color code stabilizers *directly* on the TSCC instead of computing them from the outcomes of 2-body gauge measurements. Once the color code stabilizers are measured, we decode the three copies of color code using the color code erasure decoder [15]. This decoder only needs the erasure locations as input and generates its own syndrome. We adapted it so that takes as input the previously measured syndrome and the erasure locations.

After decoding the color code copies, we lift the estimate to TSCC. After lifting we check if any logical error has oc-

curred or not. If the product of original error and the error estimate anticommutes with any one of the bare logical operators, shown in Fig. 3, we declare a logical error.

## B. Results

We present the simulation results for the TSCC derived from square octagon lattice. The TSCCs derived from the square octagon lattices have the code parameters  $[[3d^2, 2, 2d^2, d]]$ , where  $d$  is the distance of the code [4, 28]. We have simulated the proposed decoders for these codes for various erasure probabilities and lattice sizes. The gauge measurements are assumed to be noiseless. The plots shown in Fig. 20 and Fig. 21 show the variation of logical error rate with respect to the probability of erasure errors. A logical error occurs when the error and error estimate differ by a non-trivial logical operator of the TSCC. Every data point has been obtained by accumulating 2000 logical errors or 10000 runs, whichever occurs earlier.

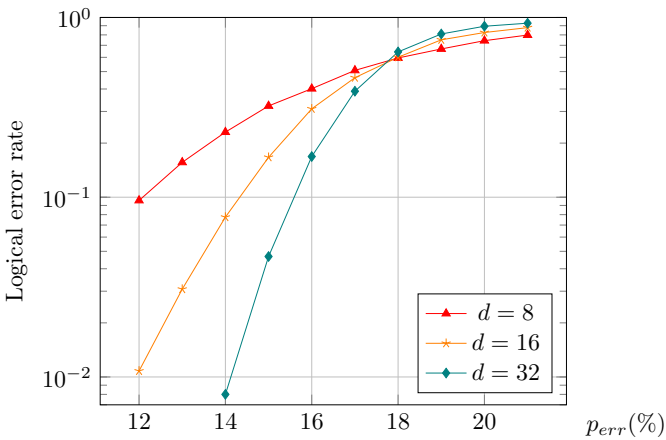


FIG. 20: Performance of partial gauge fixing decoder. Threshold is  $\approx 17.7\%$ .

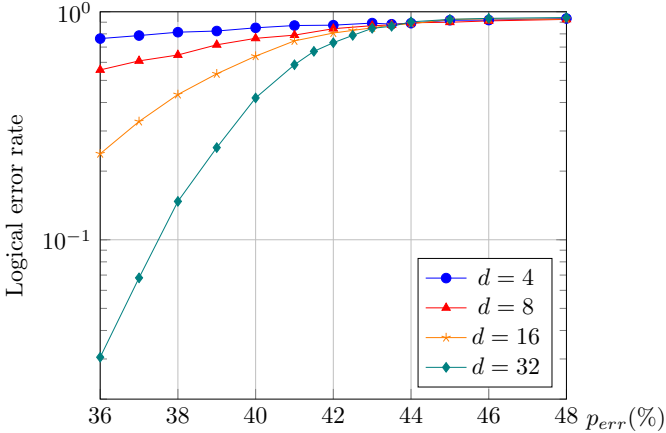


FIG. 21: Performance of the order maximal gauge fixing decoder. Threshold is  $\approx 44\%$ .

Fig. 20 shows the plot for performance of the partial gauge fixing decoder. We report a threshold of approximately 17.7%. This suggests that gauge fixing improves the performance in comparison to the highest threshold of 9.7% given in [11]. When extending to almost full gauge fixing, we observe a threshold of 44% as shown in Fig. 21. The performance of our decoder is close to 50% which is set by the no-cloning theorem.

## VIII. CONCLUSION

In this paper, we proposed two algorithms for decoding subsystem codes over erasure channel. By using the technique of gauge fixing in combination with other preprocessing techniques we were able to significantly improve the threshold of TSCCs for the erasure noise with respect to our previous work [11]. Our work draws upon the mapping of TSCC to multiple copies of color codes proposed in [5]. We decode on these color codes instead of decoding directly on TSCC which motivates in a sense the need for gauge fixing. Our first decoder uses partial gauge fixing where gauge fixing is used only to correct erasure induced bit flip errors. For this decoder we use only 2-body measurements for syndrome measurement of all the check operators. The second decoder uses maximal gauge fixing where both bit flip and phase flip errors are corrected via gauge fixing. Syndrome measurement for this decoder requires both 2-body and 4-body measurements. This keeps the advantage of subsystem code intact. The later decoder gives us a threshold of 44%. To the best of our knowledge, this is the highest threshold to date for a TSSC for erasure noise. We also formulated conditions for correctability of erasures on the subsystem codes. There remain many other interesting open questions in this context. Developing an optimal decoder without gauge fixing, improving the performance of the proposed decoders are some natural problems for further study.

*Acknowledgment.* HMS would like to thank Arun B. Aloshious for valuable discussions.

---

[1] D. Bacon, Operator quantum error-correcting subsystems for self-correcting quantum memories, *Physical Review A* **73**, 012340 (2006).

[2] D. W. Kribs, R. Laflamme, and D. Poulin, Unified and generalized approach to quantum error correction, *Phys. Rev. Lett.* **94** (2005).

[3] D. Poulin, Stabilizer formalism for operator quantum error correction, *Physical review letters* **95**, 230504 (2005).

[4] H. Bombín, Topological subsystem codes, *Phys. Rev. A* **81**, 032301 (2010).

[5] H. Bombin, G. Duclos-Cianci, and D. Poulin, Universal topological phase of two-dimensional stabilizer codes, *New J. of Physics* **14**, 073048 (2012).

[6] M. Suchara, S. Bravyi, and B. Terhal, Constructions and noise threshold of topological subsystem codes, *Journal of Physics A: Mathematical and Theoretical* **44**, 155301 (2011).

[7] V. V. Gayatri and P. K. Sarvepalli, Decoding topological subsystem color codes and generalized subsystem surface codes, in *2018 IEEE Information Theory Workshop (ITW)* (IEEE, 2018) pp. 1–5, Extended version arXiv:1805.12542.

[8] O. Higgott and N. P. Breuckmann, Subsystem codes with high thresholds by gauge fixing and reduced qubit overhead, arXiv preprint arXiv:2010.09626 (2020).

[9] N. C. Brown, M. Newman, and K. R. Brown, Handling leakage with subsystem codes, *New J. of Physics* **21**, 073055 (2019).

[10] M. Grassl, T. Beth, and T. Pellizzari, Codes for the quantum erasure channel, *Phys. Rev. A* **56**, 33 (1997).

[11] H. Solanki and P. K. Sarvepalli, Correcting erasures with topological subsystem color codes, in *2020 IEEE Information Theory Workshop (ITW) (ITW-20)* (Riva del Garda, Italy, 2021).

[12] R. S. Andrist, H. Bombin, H. G. Katzgraber, and M. A. Martin-Delgado, Optimal error correction in topological subsystem codes, *Phys. Rev. A* **85**, 050302 (2012).

[13] A. Paetznick and B. W. Reichardt, Universal fault-tolerant quantum computation with only transversal gates and error correction, *Physical review letters* **111**, 090505 (2013).

[14] H. Bombín, Gauge color codes: optimal transversal gates and gauge fixing in topological stabilizer codes, *New Journal of Physics* **17**, 083002 (2015).

[15] A. B. Alosio and P. K. Sarvepalli, Erasure decoding of two-dimensional color codes, *Phys. Rev. A* **100**, 042312 (2019).

[16] D. Vodola, D. Amaro, M. A. Martin-Delgado, and M. Müller, Twins percolation for qubit losses in topological color codes, *Phys. Rev. Lett.* **121**, 060501 (2018).

[17] N. Delfosse and G. Zémor, Linear-time maximum likelihood decoding of surface codes over the quantum erasure channel, *Phys. Rev. Research* **2**, 033042 (2020).

[18] M. A. Nielsen and I. L. Chuang, *Quantum Computation and Quantum Information* (Cambridge University Press, 2010).

[19] T. A. B. Daniel A. Lidar, *Quantum Error Correction* (Cambridge University Press, 2013).

[20] H. Bombin and M. A. Martin-Delgado, Topological quantum distillation, *Phys. Rev. Lett.* **97**, 180501 (2006).

[21] A. J. Moncy and P. K. Sarvepalli, Performance of nonbinary cubic codes, in *2018 International Symposium on Information Theory and Its Applications (ISITA)* (IEEE, 2018) pp. 334–338.

[22] A. Kulkarni and P. K. Sarvepalli, Decoding the three-dimensional toric codes and welded codes on cubic lattices, *Phys. Rev. A* **100**, 012311 (2019).

[23] N. Delfosse and G. Zémor, Upper bounds on the rate of low density stabilizer codes for the quantum erasure channel, arXiv:1205.7036 (2012).

[24] C. Vuillot, L. Lao, B. Criger, C. G. Almudéver, K. Bertels, and B. M. Terhal, Code deformation and lattice surgery are gauge fixing, *New Journal of Physics* **21**, 033028 (2019).

[25] H. P. Nautrup, N. Friis, and H. J. Briegel, Fault-tolerant interface between quantum memories and quantum processors, *Nature communications* **8**, 1 (2017).

[26] J. Haah, Algebraic methods for quantum codes on lattices, *Revista colombiana de matematicas* **50**, 299 (2016).

[27] N. Delfosse, Decoding color codes by projection onto surface codes, *Physical Review A* **89**, 012317 (2014).

[28] P. Sarvepalli and K. R. Brown, Topological subsystem codes from graphs and hypergraphs, *Phys. Rev. A* **86**, 042336 (2012).